Recent Advances in the Theory and Application of Nanofiltration: a Review

AUTHOR(S)

Y Du, B K Pramanik, Y Zhang, Ludovic Dumee, V Jegatheesan

PUBLICATION DATE

01-01-2022

HANDLE

10536/DRO/DU:30171846

Current Pollution Reports (2022) 8:51–80
https://doi.org/10.1007/s40726-021-00208-1

WATER POLLUTION (G TOOR AND L NGHIEM, SECTION EDITORS)

Recent Advances in the Theory and Application of Nanofiltration: a Review

Yuchen DU[1] · Biplob Kumar Pramanik[1] · Yang Zhang[2] · Ludovic Dumée[3] · Veeriah Jegatheesan[1]

Accepted: 11 November 2021 / Published online: 20 January 2022

Abstract
Water is the material basis for living organisms and one of the primary resources to maintain the sustainable development of the earth's ecological environment. As a water purification method, nanofiltration (NF) separation technology has been widely considered by researchers in recent years. However, most of the studies on NF in the literature focus on membrane modification, and there are only a few reviews available. In this paper, the latest research progress of NF is reviewed, and the processes of NF membrane preparation using phase inversion, layer by layer, and interfacial polymerization are described. Polymer materials used for NF membrane preparation are reviewed and the main types of nanofillers to generate thin film nanocomposite membranes, including metal organic frameworks, boron nitride, $Ti_3C_2T_X$, graphene oxide, SiO_2, and iron oxide are discussed. Membrane fouling is inevitable during NF operation and this paper analyzes the mechanisms of fouling and summarizes key pretreatment and cleaning methods required to remediate the long-term effects of cake layer formation. The steric hindrance effect, Donnan effect, and dielectric exclusion are analyzed, and some common characterization methods are summarized. The practical applications of NF are briefly introduced including groundwater, pharmaceutical wastewater, and textile wastewater treatment. Finally, the shortcomings and prospects of the existing research progress are put forward.

Keywords Nanofiltration · Rejection · Exclusion theory · Fouling · Nanomaterials

Nomenclature

API	Active pharmaceutical ingredient
ATN	Atenolol
BNNS	Boron nitride nanosheets
BNNTs	Boron nitride nanotubes
BSA	Bovine serum albumin
CA	Cellulose acetate
CECP	Cake-enhanced concentration polarization
CNTs	Carbon nanotubes
CuAAC	Copper-catalyzed azide-alkyne cycloaddition
Da	Daltons
DAB	3,3 '-Diaminobenzidine
DE	Dielectric exclusion
dGO	Deoxygenated GO
DMF	Dimethylformamide
DSPM	Donnan-steric-pore model
DSPM-DE	Donnan-steric-pore model with dielectric exclusion
DWCNTs	Double-walled carbon nanotubes
ED	Ethylenediamine
EDC	Endocrine-disrupting compounds
EMP	Emerging micropollutants
FTIR	Fourier transform infrared spectroscopy
GO	Graphene oxide
GOS	Galacto-oligosacchares
GNM	Graphene nano-mesh
HEV	Hepatitis E virus
HFPO-DA	Hexafluoropropylene oxide dimer acid
HT	Hydrotalcite
LBL	Layer by layer
MF	Microfiltration

This article is part of the Topical Collection on *Water Pollution*

✉ Veeriah Jegatheesan
jega.jegatheesan@rmit.edu.au

[1] School of Engineering and Water: Effective Technologies and Tools (WETT) Research Centre, RMIT University, Melbourne, VIC 3000, Australia

[2] School of Environmental and Safety Engineering, Qingdao University of Science and Technology, Qingdao 266042, Shandong, China

[3] Department of Chemical Engineering, Khalifa University, Abu Dhabi, United Arab Emirates

MMMs	Mixed matrix membranes
MOF	Metal organic framework
MPD	Phenylenediamine
MWCNTs	Multiwalled carbon nanotubes
MWCO	Molecular weight cutoff
NbN	Niobate nanosheet
NF	Nanofiltration
NIPS	Nonsolvent induced phase separation
NOM	Natural organic matter
ODA	Octadecylamine
OSN	Organic solvent nanofiltration
PA	Polyamide
PANI	Polyaniline
PBI	Polybenzimidazole
PC	Polycarbonate
PDA	Polydopamine
PE	Polyethylene
PEI	Polyetherimide
PEM	Polyelectrolyte multilayers
PES	Polyethersulfone
PEs	Polyelectrolytes
PhACs	Pharmaceuticals
PIP	Piperazine
PPCP	Personal care products
PSF	Polysulfone
PVDF	Polyvinylidene fluoride
PVP	Polyvinylpyrrolidone
rGO	Reduced graphene oxide
RO	Reverse osmosis
SA	Sodium alginate
S-DADPS	Disodium-3–30-disulfone-4–40-dichlorodiphenylsulfone
SDGs	Sustainable development goals
SHP	Steric hindrance pore
SiNPs	SiO_2 Nanoparticles
SWCNTs	Single-walled carbon nanotubes
TA	Tannic acid
TFC	Thin film composite
TIPS	Thermally induced phase separation
TMC	Trimethyl chloride
TOC	Total organic carbon
TSS	Total suspended solids
UF	Ultrafiltration
VSEP	Vibratory shear enhanced processing
ZCP	Zwitterionic copolymer
2D	Two-dimensional

Introduction

According to the sustainable development goals (SDGs) of the United Nations, water shortage may cause poor health conditions and affect people's livelihood and food security [1]. Today, 88 developing countries are affected by water scarcity [2]. By 2050, water scarcity may affect at least a quarter of the world's population [1]. Population growth may greatly increase the demand for agriculture [3]. However, agriculture needs to consume fresh water, which accelerates the rate of freshwater depletion [3]. For example, California's Central Valley, one of the most productive agricultural areas in the world, still faces a shortage of freshwater [4]. Therefore, groundwater has to be overdrawn to meet the irrigation demand [4]. Human activities will have a profound impact on freshwater resources. For instance, the overexploitation of groundwater has lowered the groundwater table around the world [2]. Furthermore, the production of chemicals and their release to various water and wastewater streams make pollutants appear in water at high concentrations [2]. These effects, however, are usually counterproductive to human beings. Because of the correlation between surface water and groundwater, microorganisms in surface water and pesticides, chemicals, nitrate, etc., that pollute groundwater are interrelated with each other, which eventually threaten the safety of drinking water [2].

According to World Health Organization's estimates, 502,000 people die each year because of the deterioration of drinking water [2]. Therefore, advanced water and wastewater treatment technologies such as membrane-based technologies are essential to overcome this issue.

It is generally believed that the selective barrier between two phases is membrane [5]. Membrane separation technology is widely used in water and wastewater treatment. Nanofiltration (NF) is the fourth type of pressure-driven membrane appeared after microfiltration (MF), ultrafiltration (UF), and reverse osmosis (RO) [6]. NF was first developed in the late 1970s; it is a variant of RO membrane. Usually, NF and RO are thin film composites, but NF has lower separation efficiency for smaller and less charged ions (such as sodium and chloride ions) than RO membranes [6, 7]. The separation characteristics of NF membranes are between RO and UF [8]. Compared with UF membranes, NF membranes have smaller pore sizes [8]. The molecular weight cutoff (MWCO) of the NF membrane is about 200–1000 Daltons (Da), corresponding to a pore size of 0.5 to 2 nm [6]. Compared with RO, NF membrane has the characteristics of low operating pressure and high permeation flux, so the operating cost is relatively low [7, 9]. The removal characteristics of NF are shown in Fig. 1. Figure 2 briefly summarizes the contents of this review.

Preparation of NF Membranes

The first generation of NF membranes in the early 1970s were made of cellulose acetate (CA) or its derivatives [6]. The second-generation NF film is a thin film composite

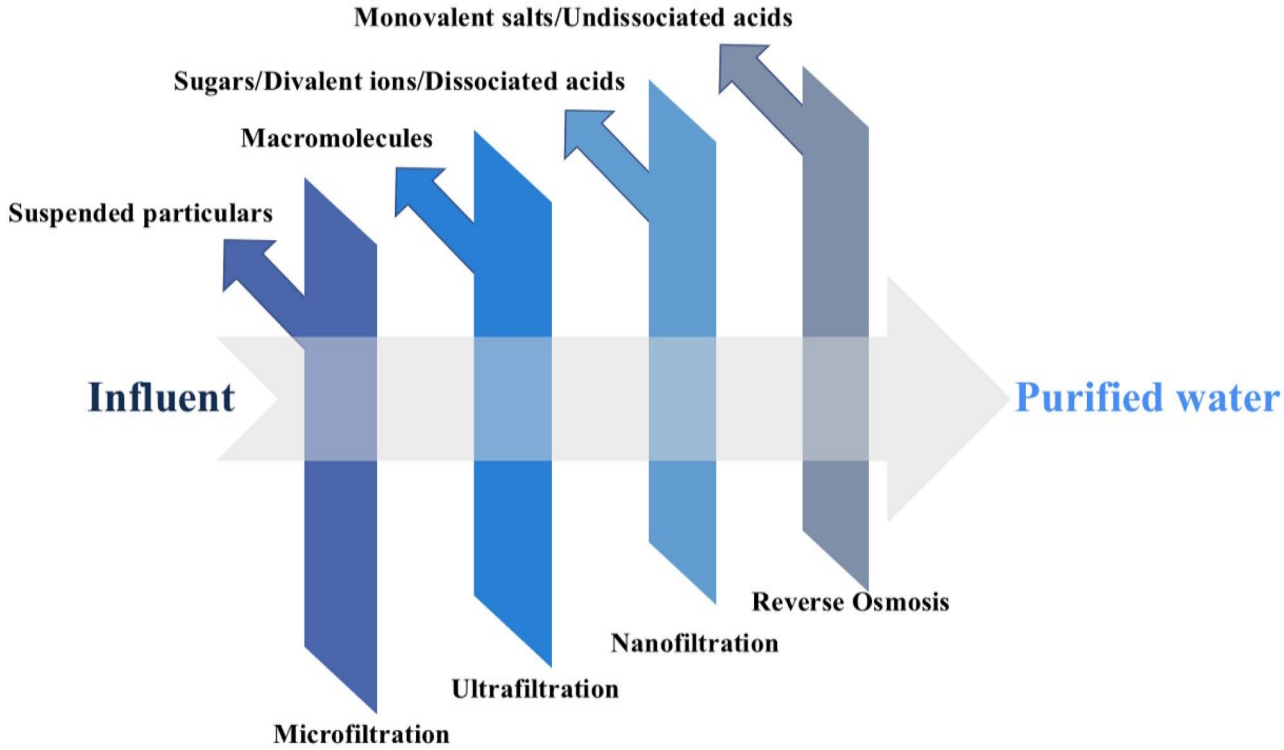

Fig. 1 Removal characteristics of four membranes

(TFC) membrane made of non-cellulose materials [6]. It consists of three different layers: an ultra-thin polyamide (PA) selective layer on the top surface, a microporous middle layer, and a non-woven polyester bottom layer [6]. The ultra-thin layer is usually composed of an amine monomer dissolved in an aqueous solution and a reactive acid chloride monomer dissolved in an organic solvent, and the two undergo a polycondensation reaction to form a PA selective

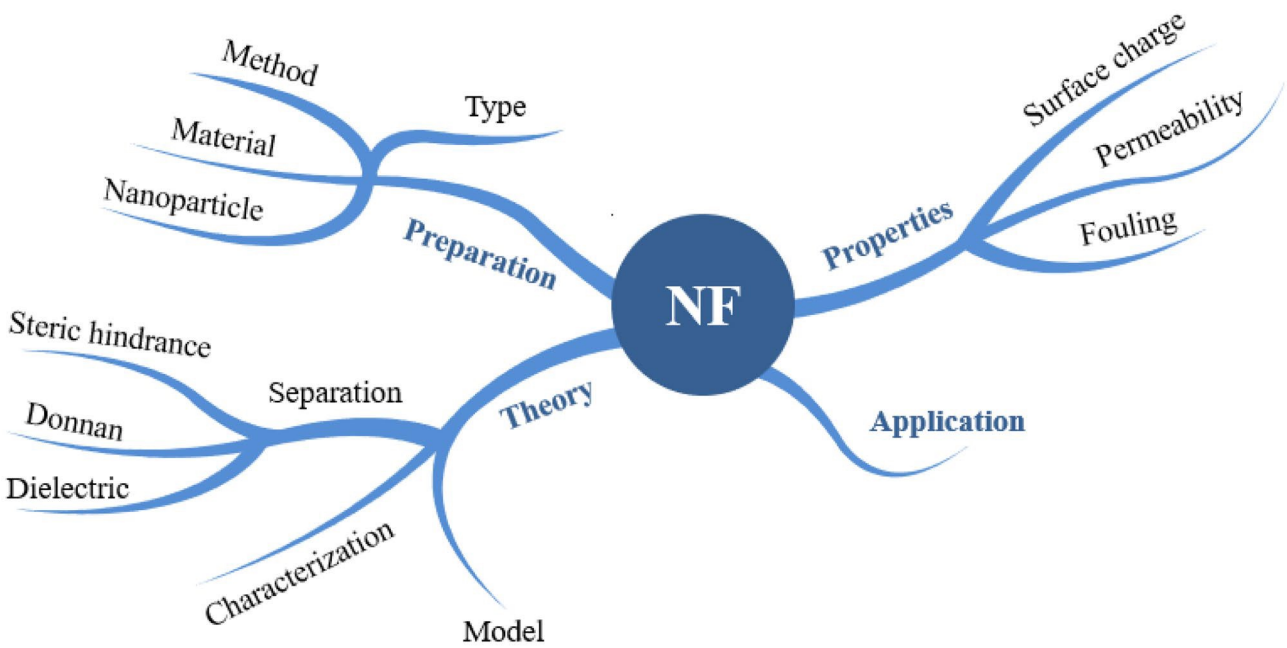

Fig. 2 Contents of NF explored in this review

layer [10]. Since 1980, CA membranes and TFC membranes have been dominating the industry [11]. Cellulose acetate membrane can work stably in harsh aprotic solvents [12]. Affinity between solute and membrane is the determinant of solute rejection in cellulose membrane, which can be regulated by carboxylic acid crosslinking [12]. CA has good hydrophilicity, biodegradability and film-forming ability. However, CA membranes are easily affected by biological and organic pollutants [13]. NF membranes usually have an asymmetric structure and are supported by a thick polymer barrier layer (CA, PA, sulfonated polysulfone) [8].

Method of Preparation

In this section, the preparation of nanofiltration membrane by phase inversion, layer by layer, and interfacial polymerization is discussed.

Phase Inversion Method

The preparation of OSN membrane by phase inversion method has always been an important subject. Manufacturing of OSN membranes usually involves using either nonsolvent induced phase separation (NIPS) or thermally induced phase separation (TIPS) technologies [14]. The comparison between NIPS and TIPS is shown in Table 1.

The core of phase inversion method is to transform polymer from liquid to solid [5]. Because of simple operation, most of phase inversion membranes use immersion precipitation method [6]. That is, the polymer solution is scraped on the support, immersed in a coagulation bath containing a non-solvent, and precipitated due to the exchange of the solvent and the non-solvent [5]. The structure of the formed membrane is determined by both mass transfer and phase separation [5]. According to the target properties of the membrane, the membrane can be modified and post-treated. Most of the polymer membranes used in OSN require post-treatment cross-linking technology. In general, the chemical cross-linking of polymer chains improves the performance of the membrane by avoiding the reduction of membrane flux due to the compression of polymer chains or the swelling of the polymer matrix under the action of organic solvents [17]. For instance, increasing the crosslinking degree of PA layer can form highly hydrophilic membrane [18]. After cross-linking with (3-glycidyloxypropyl) trimethoxysilane, the chemical stability of the polythiosemicarbazide NF membrane prepared by the phase inversion method is significantly improved [17]. This can be attributed to the organic–inorganic network (-Si–O-Si-) formed by cross-linking [17].

Layer by Layer (LBL)

LBL method is alternating electrostatic adsorption of cation and anion polyelectrolytes (PEs) on the surface of a UF membrane [6]. During the preparation process, the charged porous UF substrate is alternately immersed in a solution containing cationic and anionic PEs, which usually reverse the surface charge, and subsequent deposition can form a layered composite, the so-called self-assembly PE complex [6, 19]. The deposition time affects the separation performance of the LBL membrane. As the deposition time increases, the water permeability of the membrane is decreased. This may be because the thickness of the layer increases with the increase of the deposition time, resulting in an increase in the impermeability of the membrane [19]. The problem of LBL method in engineering application is that it takes a lot of time to fabricate multilayer films [19]. Because of this, dopamine materials attract researchers' attention. In the process of dopamine self-polymerization,

Table 1 Comparison of NIPS and TIPS

	Methods	
	NIPS	TIPS
Preparation process	At first, the homogeneous coating solution is prepared by dissolving the polymer in a suitable solvent, then casting the prepared solution onto the substrate to prepare a film, and then immersing the film in a non-solvent bath (usually water) to solidify [14]	Prepared at high temperature, the film is formed by cooling the as-cast solution below its freezing point [14]
Characteristics	A large amount of wastewater with solvent is produced [14] This is because the curing of polymer is caused by the reduction of free energy due to the mixing of non-solvent and solvent [15]	Energy consumption is relatively high This is because the polymer needs to be dissolved in the diluent at high temperature and phase separated during cooling [16]
Common used polymers	Polysulfone (PSF), polyethersulfone (PES), polyvinylidene fluoride (PVDF)	PA, polyacrylonitrile
Common used solvent	N-Methyl-pyrrolidone, dimethylacetamide, dimethylformamide (DMF)	Polyethylene glycol

catechol and amino group in dopamine molecule play a leading role [19]. Therefore, some researchers believe that simulating catechol and amino group at the same time can replace dopamine [19]. Tannic acid (TA) and Jeffamine can replace dopamine [19]. Jeffamine is a hydrophilic compound similar to polyethylene glycol [19]. Guo et al. [19] found that the hydrogen bond in Jeffamine can interact with the hydroxyl group in TA and promote the LBL process. The water contact angle of the prepared membrane decreased from the initial 55° to 44.5° [19]. This is due to the covalent reaction between amino group in Jeffamine and quinone group in TA, and the hydrogen bonding reaction between phenolic hydroxyl group and ether group, which improves the hydrophilicity of the membrane [19].

Troger's base polymers are a special type of intrinsic microporous polymers, which can be used to enhance the stability of NF membranes [20]. Agarwal et al. [20] used Troger's base polymers to prepare NF membranes by the LBL method. The membrane has good stability in acid, alkali, and other harsh environments, which may be due to the structure of Troger's base and the interaction of hydroxyl groups in Troger's base [20]. Hydroxyl groups can participate in the cross-linking reaction and enhance the solubility of the polymer in polar solvents, while Troger's base has a rigid structure, which is conducive to improving the stability of the membrane [20].

Polyelectrolyte multilayers (PEM) can also be used to enhance the stability of NF membrane. PEM are driven by the electrostatic interaction between opposite charged PEs and the entropy increases of PEs release counter ions and hydrated molecules [21]. Ordinary NF membrane undergoes hydrolysis under extreme pH conditions. In contrast, PEM can still maintain stable performance. PEM NF membranes prepared by LBL method have the advantages of high permeability and adjustability [22]. This may be because when LBL method is used, ionic strength, polyelectrolyte type, and pH value can be adjusted to control the performance of PEM materials [22]. Adjusting the polyelectrolyte and salt concentration of LBL can also change the pore structure of PEM membrane and enhance the selectivity of membrane [21].

Interfacial Polymerization

Another way to prepare NF membrane is interfacial polymerization. The interfacial polymerization method can form an ultra-thin selective PA layer with a thickness of hundreds of nanometers on the surface of the microporous support membrane, thereby preparing a TFC membrane with good water flux and solute retention [6]. The essence of interfacial polymerization method is to control the polymerization process to form a polymer network on the porous substrate at the interface of two immiscible phases [23]. Duong et al. [24] used the interfacial polymerization method and polyetherimide (PEI) as the support layer to synthesize zwitterionic copolymer (ZCP) membrane. The organic solution of n-hexane containing trimethyl chloride (TMC) was polymerized with the aqueous solution of ZCP/phenylenediamine (MPD) [24]. Finally, deionized water is used to remove the excess chemical substances and the membrane can be formed after drying [24]. After cross-linking MPD and PEI, the newly prepared membrane has a thicker and denser selective layer than the original film [25]. The density of the active layer increases the dye rejection, but the membrane flux decreases with the increase of mass transfer resistance [25].

Ormanci-Acar et al. [26] used TMC in the organic phase and disodium-3–30-disulfone-4–40-dichlorodiphenylsulfone (S-DADPS)/piperazine (PIP) in the aqueous phase to fabricate NF membrane by the interfacial polymerization method. The preparation method is roughly divided into 3 steps. They are as follows: (a) prepare the aqueous phase solution of PIP/S-DADPS and the organic phase solution of TMC, (b) immerse the support film saturated with the aqueous phase solution into the organic phase solution, and (c) heat setting for the membrane and wash it with deionized water [26].

When using interfacial polymerization, the choice of reaction monomer is the key factor affecting the properties of NF membrane. For instance, Das et al. [27] used water and n-heptane as solvent, using interfacial polymerization, to synthesize a covalent organic triazine-PIP based membrane on a polyacrylonitrile carrier. Pure water flux of the membrane is 138.7–142.5 $Lm^{-2}\ h^{-1}\ bar^{-1}$, which is higher than 65 $Lm^{-2}\ h^{-1}\ bar^{-1}$ of commercial NF270 [27, 28]. This can be attributed to the condensation reaction between the triazine part of cyanuric chloride and PIP, forming a network structure [27].

Other Preparation Methods

Solvent activation is a method to change the performance of RO membrane by solvent post-treatment [29]. NF can also be prepared by solvent activation of RO. The structure of common PA NF membrane is easy to destroy under an acidic condition, and the acid resistance of NF membrane prepared by solvent activation method will enhance the stability of the membrane [7]. Shin et al. [7] prepared a RO level m-MPD base membrane on a porous polyethylene (PE) carrier. They modified the membrane by deforming the PA network through highly soluble polar aprotic solvents. Compared with the commercially available NF270 membrane, the prepared NF membrane has a 30% increase in water permeability, enhanced acid resistance, and an ion selectivity of 6.8 times that of NF270 [7]. This is because polar aprotic solvents make the initial RO membrane swell, PA structure is loose, and the membrane performance changes from RO level to NF level [7].

Click chemistry is the rapid chemical synthesis of molecules by splicing them into small units, which can be used to produce highly cross-linked and chemically stable polymers [23]. Kyriakou et al. [23] prepared Al-SiM/TE membrane on a ceramic carrier by interfacial polymerization and two successive sulfur-bromine click reactions. Al-SiM/TE membrane still has stable water permeability at 150 °C [23]. Compared with the conventional interfacial polymerization method, the new method can save at least 90% of raw materials [23]. Hoffman and Phillip [30] used NIPS and copper-catalyzed azide-alkyne cycloaddition (CuAAC) click reaction to develop a dual-function NF membrane. The mechanism of bifunctional NF membrane is similar to that of Janus membrane, both of which have asymmetric structures or properties [30]. After immersion in bovine serum albumin (BSA) solution and rinsing with water, the flux of bifunctional NF membrane can be restored by 99%, while that of ordinary NF membrane can only be restored by 65% [30]. This shows that the dual-function NF membrane has strong antifouling ability.

3D printing is a technology based on material deposition [31]. At present, it is widely used in industries such as simple models creation, advanced art, and even aircraft parts production [31]. 3D printing can also be applied to the preparation of NF membrane. Park et al. [32] used 3D printing technology to add honeycomb spacer into NF membrane. Compared with the empty channel membrane, under the condition of high pollution, the flux is increased by 26.4% due to the existence of honeycomb spacer [32]. They speculated that the enhancement of antifouling ability was related to the unique antifouling layer of honeycomb spacer. Different NF preparation methods are listed in Table 2.

Common Materials used in the Synthesis of NF Membrane

Reactive Monomers

The performance of the membrane depends on the chemical properties of reactive monomers, additives, and accelerators [27]. The additives may be monomers, catalysts, surfactant, co-solvents, or inorganic particles involved in the reaction [33]. Common monomers include acyl chloride, TMC, MPD, and PIP and its derivatives [27]. The PA membrane cross-linked by MPD and TMC is widely used in commercial NF membrane [6].

The crests and troughs on the selective layer of the membrane are generally considered to be affected by the equilibrium of reaction rates between diamines and acyl chlorides, and the dispersion rate of diamines from aqueous phase to organic phase [34]. The crests and troughs affect the membrane surface roughness. Generally, the higher the surface roughness of the film, the more susceptible the film is to be fouled [35].

New monomers such as diamine containing sulfonic acid, diamine containing tertiary amino group, and diamine containing ethoxy group have been synthesized [36]. Ji et al. [36] used a new monomer 3,3 '- diaminobenzidine (DAB) for the preparation of NF membrane. The rejection rate of Na_2SO_4 by the membrane prepared by cross-linking reaction of DAB and TMC can reach 84.2% [36].

Substrate Materials

Polybenzimidazole (PBI) can be used for high temperature filtration due to its high glass transition temperature of 410–430 °C [37]. Membranes made of PBI can be modified with TMC to enhance chemical stability. The secondary amine on the imidazole ring of PBI reacts with the acid chloride of TMC to form a tertiary amine group [38]. The interaction between PBI and sulfuric acid can also be used for membrane modification. Each PBI repeat unit may react with two sulfuric acid molecules to form a highly entangled polymer network [37]. After the reaction, the solvent resistance of the membrane is enhanced due to the existence of hydrogen bonds [37].

Other commonly used NF membrane polymer materials are PEI, PSF, PES, and PVDF. Among them, PSF has received extensive attention due to its chemical stability and

Table 2 A simple summary of different NF preparation methods

Type	Mechanism
1. Phase inversion	Phase transition of polymer
1.1 NIPs	Immersion precipitation
1.2 TIPs	Polymer is dissolved in solvent at high temperature and phase separated during cooling
2. LBL	Alternating electrostatic adsorption polyelectrolyte
3. Interfacial polymerization	Polymerization carried out at two incompatible interfaces
4. Solvent activation	RO membrane swelling by polar aprotic solvents
5. Click chemistry	Click reactions
6. 3D printing	Material deposition

non-toxicity [39]. Generally, PSF is made by the reaction of diphenol and bis (4-chlorophenyl) sulphone [39].

The membrane prepared by PEI has high rejection of divalent cations and anions [40]. However, the adsorption of PEI is poor [40]. This problem can be improved by adding surfactants. For example, after adding sodium dodecyl sulfate, the hydrophilicity and surface charge of the membrane increased, and the rejection rate of $MgCl_2$ reached 93% [40]. Surfactant can enhance the affinity between amine and membrane carriers and reduce the interfacial tension between water and organic solvent [40].

PVDF is a kind of hydrophobic polymer material [41]. Due to the stability of PVDF, it can be used in extreme conditions [42]. PVDF is easy to be fouled by protein, resulting in the decrease of water flux [41]. PVDF needs to be modified with other materials to enhance its hydrophilicity.

The hydrophilicity and complexing ability of PVDF can be improved by blending amphiphilic copolymer with PVDF [41]. Inorganic nanoparticles can interact with polymer surface to enhance the performance of the membrane. Mahdavi et al. [41] added hydrophilic copolymer PVDF-g-polyvinylpyrrolidone (PVP) and nanoparticle TiO_2 to PVDF film. Compared with pure PVDF membrane (64.21%), the new membrane had higher rejection rate (95.35%) of bovine serum albumin solution [41].

The NF membrane formed by cross-linking PVDF with aliphatic amines has a short cross-linking time, and after soaking in 5 M HCl or NaOH for 5 days, the retention rate does not change significantly, indicating that the membrane is suitable for extreme pH environments [43]. If the crosslinking time of PVDF is too long, the thermal stability and mechanical stability of the membrane may be affected [42].

Green Organic Materials

Sodium alginate (SA) is a by-product of iodine and mannitol extracted from brown algae kelp or *Sargassum*, composed of 1–4-hydroxy-D-mannuronic acid (M) and α-L-guluronic acid (G) [44]. Crosslinked SA can improve the chemical stability of the membrane. The SA composite membrane prepared by phase separation technology has solvent resistance to dimethylformamide and dimethyl sulfoxide [44].

Plant polyphenols are plant-derived phenols, and TA is one of them. Plant polyphenols are water-soluble substances widely existing in trees, fruits, and vegetables, which can protect plants from microorganisms, insects, and even ultraviolet radiation [45]. Taking plant polyphenols with antioxidant activity is beneficial to the human body [45]. The crosslinking of TA and polyacrylonitrile is used to prepare NF membrane. After crosslinking, due to the reduction of space between polymer chains, the bearable tension of fiber increased, and TA can penetrate into substrate, so mechanical properties of the membrane are improved [45]. An overview of commonly used materials for NF preparation is shown in Table 3.

Nanoparticles

Mixed matrix membranes (MMMs) are organic membranes modified by adding inorganic materials. The prerequisite for forming MMMs is that inorganic materials have groups that are easy to react with polymer chains [17]. The introduction of nanomaterials can control the membrane pore size through nanochannels to enhance the steric hindrance effect [46]. Nanomaterials can also enhance the hydrophilicity of the membrane. In general, the hydrophilic membrane has good antifouling ability [47]. The atomic thickness and transverse dimension of two-dimensional (2D) nanosheets are from submicron to several micrometers, with a large specific surface area and solid properties [82]. Typical 2D nanosheets are metal organic framework (MOF), boron nitride, $Ti_3C_2T_X$ (MXene), and graphene oxide (GO).

Metal organic Frameworks (MOF)

MOF, a highly crystalline porous material, is easier in controlling the membrane pores at the molecular level than other inorganic nanofillers [10]. The unique pore structure, chemical function, and high specific surface area make MOF a new research direction in seawater desalination [10]. MOF's research on NF includes ZIF-8, ZIF-93, MIL-53, and UIO-66 [10, 48]. The properties of the membrane are affected by the wide specific surface area and chemical properties of the MOF [48]. For example, the aldehyde group in ZIF-93 can form Schiff bases with the amine group in the reactive monomer [48]. The water permeability of PA-ZIF-93 membrane is about 0.18 $Lm^{-2}\ h^{-1}\ bar^{-1}$ higher than that of ordinary membrane [48]. This may be due to the change of hydrophilicity and crosslinking degree of the membrane due to the addition of ZIF-93 [48]. The crystal structure of ZIF-8 can enhance the membrane stability. The rejection rate of Na_2SO_4 and pure water permeability of ZIF-8 NF membrane with TA-Zn^{2+} as zinc source remained stable within 100 h of operation [49]. SEM and ATR-FTIR showed that the structure of the membrane does not change significantly, indicating that the membrane structure is stable [49]. This may be due to TA further enhancing the reaction between ZIF-8 and substrate [49].

Boron Nitride Nanomaterial

Hexagonal boron nitride is used as boron nitride nanomaterials, which is the most stable of the four crystal forms [50]. It has high chemical stability (in a wide range of acids and

Table 3 Commonly used materials for NF preparation

Type	Chemicals	Chemical formula	Molecular weight of structural unit	Properties	CAS
Reacting monomers	TMC	$C_9H_3Cl_3O_3$	265.48	Stimulate the eyes, skin, and respiratory tract	4422–95-1
	MPD	$C_6H_8N_2$	108.14	Dissolve in water Acute toxicity: rat oral LD_{50}: 650 mg/kg	108–15-2
	PIP	$C_4H_{10}N_2$	86.14	Dissolve in water, combustible, corrosion, irritation	110–85-0
	DAB			Unstable at room temperature Potentially mutagenic	
Substrate	Polyimide	$C_{35}H_{28}N_2O_7$	588.61	Insoluble in organic solvents	62929–02-6
	PA	$C_{18}H_{35}N_3O_3$	341.49	Heat and chemical resistance	63428–83-1
	Polyacrylonitrile	$(C_3H_3N)n$		Insoluble in water	25014–41-9
	PBI	$C_7H_6N_2$	118.14	Solvent and chemical resistance	25928–81-8
	PEI	$C_{37}H_{28}N_2O_8$	628.62	Heat and chemical resistance	61128–46-9
	PSF	$C_{27}H_{26}O_6S$	478.56	Nontoxic	25135–51-7
	PES	$(C_{12}H_{10}O_4S\cdot C_{12}H_8Cl_2O_2S)n$		Heat resistance	25608–63-3
	PVDF	$(CH_2CF_2)n$		Heat and chemical resistance	24937–79-9
Green organic materials	SA	$C_6H_7O_6Na$	216.12	Insoluble in organic solvents	9005–38-3
	Bentonite clay	Al_2O_3 $4(SiO_2)H_2O$	360.31	nontoxic	1302–78-9
	TA	$C_{76}H_{52}O_{46}$	1701.20	Acute toxicity: mouse intravenous LC_{50}: 130 mg/kg	1401–55-4

bases) and temperature stability (up to 900 °C) [50]. The permeability and antifouling ability of the NF membrane can be enhanced by adding boron nitride nanomaterials. Adding 0.05 wt% of boron nitride nanosheets (BNNS) to the PES substrate can increase the pure water permeability of the NF membrane by 4 times, the rejection rate of humic acid reaches 95%, and the flux recovery rate is 100% [50]. The NF membrane made by introducing boron nitride nanotubes (BNNTs) into the PA thin film selective layer has increased the permeability of pure water by 4 times compared with ordinary NF membranes [51]. This is because the addition of boron nitride nanotubes increases the water transmission channel. However, when the content of BNNTs is too high (> 0.02wt%), the overall performance of the membrane decreases due to the agglomeration of BNNTs [51].

$Ti_3C_2T_X$ (MXene)

$Ti_3C_2T_X$ (MXene) is a 2D nanosheet, which can be used to increase the rejection rate of CA membrane and increase the effective negative charge and hydrophilicity. The increase in rejection rate is due to the formation of smaller pores and reduction of macrovoids when MXene is cross-linked with the CA base membrane [13]. With the addition of MXene, the water contact angle decreased from 70.3° to 54.0° [13]. Due to the negative surface of the MXene film, compared with the normal CA membrane (−24.84 mV), the MXene membrane has more negative zeta potential (−32.42 mV) [13].

Graphene Oxide (GO)

GO has a 2D hexagonal honeycomb structure, which is composed of sp^2 carbon atoms [52]. GO membrane has good molecular sieve performance, water permeability, flexibility, and surface hydrophilicity [53]. GO is rich in oxygen functional groups (hydroxyl, epoxy, and carboxyl) and easy to form hydrophilic structure with polar molecules [53, 54]. The structure of the nanosheets is conducive to solvent exchange [54]. Compared with MXene, the synthesis of GO is easier [55]. However, the interaction between GO sheets makes the graphene-based membrane compact, which is harmful for the permeability of the membrane [54]. GO membrane has poor structural stability in water environment. When GO is hydrated, membrane is negatively charged, and it is usually decomposed. This is likely due to electrostatic repulsion [56]. These problems can be mitigated by reducing GO to reduced graphene oxide (rGO) to enhance the van der Waals interaction between sheets or crosslinking of small molecules with oxygen-containing GO groups [57].

The nanohybrid TiO_2@rGO has both the hydrophilicity of TiO_2 and the solvent channelization of GO [54]. The introduction of TiO_2@rGO to NF membrane raised the flux

of polar solvent (ethanol flux increased by 59%) and reduced the flux of nonpolar solvent (n-hexane flux decreased by 10%) [54]. The NF membrane formed by the hybrid of graphene oxide nanoribbon (GONR) and rGO has an ultra-high water permeability of 312.8 Lm^{-2} h^{-1} bar^{-1} due to the expansion of nanochannels [57]. Octadecylamine (ODA) functionalized rGO can make the nanofillers more hydrophobic than GO, which is beneficial to the dispersion in the organic phase of interfacial polymerization. The permeability of NF membrane with rGO-ODA is 35–54% higher than that of unmodified PA membrane [52]. Sodium niobate nanosheet (NbN) can be used to modify GO to enhance the water permeability of the film by increasing the channel [53]. Kim et al. [55] treated GO with NaOH to get deoxygenated GO (dGO). The d-spacing of graphene layer is very important to allow solvent and small molecules to penetrate and prevent molecules larger than the d-spacing [55]. Kim et al. [55] found that the d-spacing of dGO (7.6 Å) is smaller than that of GO (9.2 Å). After soaking in water for 1 day, the d-spacing of GO increased to 13.4 Å, while dGO remained unchanged, which indicated that NaOH treatment could enhance the interaction between nanosheets [55]. The stability of GO membrane can be improved by crosslinking with diamine monomer. This is due to the formation of new N–H covalent bond by condensation and nucleophilic substitution between amino group and GO sheet, which prevents the membrane from disintegrating [56]. The NF membrane modified by GO and hexanediamine has good chemical and mechanical stability, which is suitable for acetone and other organic solvents [58].

In addition, Nam et al. [59] studied the effect of carrier morphology on the properties of the GO-based membrane. They also produced folds on polycarbonate (PC) substrates by argon ion bombardment. Ion beam treatment can change the surface morphology of PC carrier without affecting the properties of polymer carrier [59]. The permeability of GO is increased by 6.4 times on PC carrier with more folds [59]. This is due to the wrinkle of porous support, which makes the GO layer spacing larger than the GO layer spacing on the flat surface [59]. The increase of interlayer spacing provides a larger channel for water molecules [59].

SiO_2 Nanoparticles (SiNPs)

Crystalline and amorphous are two forms of silica [33]. Crystalline silica is harmful to the human body. Amorphous silica is widely used in the food, beverage, and cosmetics industry [33]. SiNPs belong to amorphous silica. Alhumaidi et al. [60] used SiNPs/poly (L-DOPA) (3-(3,4-dihydroxyphenyl)-L-alanine) to synthesize antifouling layer on the surface of NF membrane. They found that the antifouling layer can increase the hydrophilicity of the membrane, reduce the surface roughness, and decrease microbial population growth by 50% [60]. Polydopamine (PDA) can strongly adhere to the surface of materials [61]. Ang et al. [61] used this property to graft silica nanoparticles with PDA to form PDA-SiNPs on top of the substrate. PDA-SiNPs were used to modify the PA membrane. The results showed that the flux of the modified membrane increased by 91.1% and had a certain antifouling ability [61]. The increase of antifouling ability is due to the increase of fouling resistance and critical flux due to physical surface modification [62]. The high polar main chain of PDA is beneficial to the compatibility with other molecules and enhancement of the hydrophilicity of the membrane [63]. For example, PDA can be grafted with PEI rich in cationic amino groups to improve the hydrophilicity of the membrane [64]. After modification, the contact angle of the film decreased from $55° \pm 1.5°$ to $46.7° \pm 3.7°$ and the charge density increased [64]. Except SiO_2, the high adhesion of PDA can also be used for other nanoparticles. For example, ZnO nanoparticles were assembled into commercial NF membranes by rapid deposition of PDA, and the membranes exhibited antibacterial activity against *Bacillus subtilis* [65]. This may be due to the ability of Zn^{2+} ions to penetrate and deconstruct the cell wall of *Bacillus subtilis* [65]. Ang et al. [33] used silica spheres to modify PSF membranes. The water contact angle of the modified PSF membrane is $20.4 \pm 1.4°$ compared with that of the original PSF membrane ($39.6 \pm 2.2°$), which indicates that the hydrophilicity of the modified PSF membrane is improved [33].

Fe_3O_4/FeO

Fe_3O_4 is hydrophilic, magnetic, and chemically stable [47]. Fe_3O_4 agglomerates easily in organic solvents and is sensitive to oxidation [66]. This problem can be solved by immobilizing reactive ligands on the surface of nanoparticles and using surface coating with adsorption layer [47]. Compared with the ordinary PES membrane, the surface of modified membrane was smooth and the tensile strength was improved after adding Fe_3O_4/PVP nanoparticles [47]. Using amorphous silica (95.55%) as the protective layer of Fe_3O_4 magnetic nanoparticles can enhance the dispersibility and chemical stability of Fe_3O_4 [66]. Embedding Fe_3O_4@SiO_2-NH_2 into the PES membrane, the pure water flux of the membrane increased by 23 Lm^{-2} h^{-1}, and the removal rate of cadmium Cd(II) ion reached 93% [66].

FeO nanoparticles have the advantages of a large specific surface area, low price, and hydrophilicity [67]. They are commonly used in water treatment, land cleaning, sensors, and environmental remediation [67]. The addition of FeO nanoparticles can effectively improve the physical and chemical properties of the membrane and reduce the membrane pollution [67]. The water contact angle of NF membrane with FeO decreased from 84.7° to 49.6° and the

flux recovery was 81.16%, which was higher than 50.16% of common membrane [67].

Other Nanoparticles

Hydrotalcite (HT) is an anionic clay compound with unique physical and chemical properties [68]. HT is rich in hydroxyl groups and is non-toxic. After being modified with HT, the number of pores on the membrane surface increased, the rejection rate of Pb^{2+} increased by 20.7%, and the water contact angle decreased due to the presence of hydrophilic functional groups [68]. Silver ion exchange zeolite has bactericidal ability, which can be attributed to the fact that many charge sites on the surface of zeolite can be used for ion exchange to release Ag^{+} [69]. The composite membrane containing silver ion exchange zeolite showed complete inactivation of *Escherichia coli* in 210 min [69]. Bentonite clay is a naturally occurring silicon-aluminum layered silicate with a unique tetrahedral structure [70]. The water contact angle of the PA membrane with sulfonated bentonite is 50.125° and that of the common PA membrane is 66.35°, which indicates that sulfonated bentonite is beneficial to improve the hydrophilicity of NF membrane [70].

Inorganic Materials

In addition to the abovementioned organic membranes and MMMs, inorganic membranes have gradually been favored by researchers. Inorganic membranes have long-term chemical and thermal stability and high mechanical strength [11]. The disadvantages of inorganic membrane are high cost and brittleness [56]. Inorganic membranes generally include metal oxide membranes and carbon-based membranes. The details of different types of inorganic materials–based NF membrane are discussed in the following section.

Metal Oxide Membrane

The most commonly used method for preparing metal oxide ceramic membranes is the sol–gel method, which is usually divided into 4 steps. They are as follows: (a) the precipitation reaction occurs between the hydrolyzed precursors; (b) the peptization reaction, where the precipitation is converted into colloidal sol; (c) the stable sol is coated on the porous carrier and forms a gel during the drying process; and (d) the membrane is sintered at a high temperature to optimize its mechanical properties and pore structure [11]. Commercial metal oxide films and inorganic membranes generally use alumina (Al_2O_3), zirconia (ZrO_2), and titania (TiO_2) [11].

In the preparation of ceramic membranes, alumina is often combined with other more stable oxides, such as ZrO_2, due to its low chemical stability [71]. There are many kinds of crystal phases in Al_2O_3, among which α-Al_2O_3 and γ-Al_2O_3 are often used in the preparation of membranes [72]. γ-Al_2O_3 membrane has a pore size in the range of UF and is unstable in acidic solution, so it is often used in gas separation [72]. Anisah et al. [72] prepared NF membranes on porous α-Al_2O_3 carriers at 200 ℃. However, with the sintering temperature increasing from 200 to 500 ℃, the pore size of the membrane increased [72].

The use of microporous materials to modify ceramic membranes has received much attention in recent years. Adding microporous polymer frameworks to the alumina ceramic membrane can enhance the permeability of organic solvents. For example, the thickness of selective layer of α-alumina membrane modified by porous organic framework is reduced by 40 nm, which promotes the improvement of membrane permeability [73].

Anisah et al. [74] studied the thermal stability of TiO_2-ZrO_2 NF membranes. The results show that the water permeability and MWCO of the membrane change only in the initial 20 h, and then remain stable [74]. The disadvantage of TiO_2-ZrO_2 NF film is that the crystalline parts of TiO_2 and ZrO_2 are so dense that the molecules cannot be transported [75]. The effective voids on the membrane for permeation are the crystal boundaries, and it is difficult to finely control the size and increase the effective void space [75]. Sada et al. [75] used organic chemical ligand (OCL) templated TiO_2-ZrO_2 NF membrane. During the preparation process, OLC was completely decomposed, and the prepared membrane had a larger specific surface area and micropores [75]. Similarly, mixing the two materials can reduce the costs as well. For example, if only ZrO_2 is used, although the filtration performance of the membrane is good, it is not practical because of its high cost [71]. The rejection rate of ZrO_2 NF membrane doped with yttrium oxide to furan is up to 89% [76]. The enhancement of the rejection performance is due to the inhibition of tetragonal monoclinic phase transition of ZrO_2 film by yttrium oxide, which improves the integrity of the membrane [76]. Nanowire-based porous membranes made of TiO_2 and Al_2O_3 have a pore size range of 5–500 nm and a porosity of 70% [77]. Modification of the porous membrane with silicone oil can obtain a non-porous NF membrane, which has high methanol permeability [77].

Carbon-Based Membrane The materials used in carbon-based membranes are ordered mesoporous carbons such as carbon nanotubes (CNTs) and graphene [11]. Among them,

CNTs are divided into single-walled carbon nanotubes (SWCNTs), double-walled carbon nanotubes (DWCNTs), and multiwalled carbon nanotubes (MWCNTs) [11].

CNTs have the characteristics of fast water transmission and low curvature, which reduce the friction of water on the defect-free carbon surface in the nanotubes [51]. CNTs can be used to improve the upper limit between selectivity and permeability balance of polymer membranes [78]. Compared with BNNTs, CNTs are more suitable for improving the water flux of the membrane. This is likely due to the difference in the electronic landscape in the nanotube wall [51]. Compared with normal PSF NF membrane, the pure water permeability of the membrane modified with 0.5% CNTs is nine times higher than that of the original membrane [79].

The conductivity of polyaniline (PANI) contributes to the electron conduction between CNTs. Based on this, PANI/CNT NF membranes were prepared by Zhang et al. [80]. They found that PANI can increase the charge density of the film' to 'Since PANI can increase the charge density of the membrane, when the applied voltage increases, the electrostatic interaction between membrane and ions is enhanced; the rejection rate of Na_2SO_4 increases from 81.6 to 93.0%; and the rejection rate of NaCl increases from 53.9 to 82.4% [80]. Another study is by Yang et al. [81] who studied a graphene nano-mesh/single-walled carbon nanotube (GNM/SWCNT) hybrid film. This kind of membrane has good mechanical properties and can withstand large deformations [81]. The high mechanical strength can be attributed to the π-π interaction between SWCNT and GNM [81]. SWCNT was used as the intermediate layer between PA active layer and PES substrate by inkjet printing technology [82]. The rejection rate of NF film to Na_2SO_4 was 97.88% [82]. This may be due to the formation of a buffer layer after SWCNT covers the PES substrate, which makes the monomers uniformly diffuse and forms a PA layer with a high crosslinking degree [82].

The shortcoming of MWCNTs is self-aggregation and poor compatibility with polymer matrix [83]. The performance of MWCNTs is usually enhanced by introducing hydrophilic functional groups. β-Cyclodextrin functionalized MWCNTs have a rejection rate of 92% for Direct Red 16, a flux recovery rate of 89%, and an improved antifouling performance [83]. MWCNTs functionalized with ethylenediamine (ED) can reduce the interaction between PES and solvent molecules in the process of membrane formation, thus forming larger membrane pores, which helps improve the pure water flux [9]. The water flux of the NF membrane modified by carboxylated carbon nanotubes COOH-MWCNTs was increased by 30%, and there was no "trade-off" between permeability and selectivity [78]. Tables 4 and 5 respectively list the nanoparticles used in NF manufacturing in recent years and their preparation methods.

Types of NF Membranes

There are usually two types of NF membranes such as flat sheet membranes and hollow fiber membranes. Commercial NF membranes are flat membranes because the current production process of composite membranes is only suitable for flat membranes [90]. Most commercial NF membranes are manufactured using interfacial polymerization [90]. Hollow fiber membrane has the potential to replace flat membrane in the future. Hollow fiber membrane has the advantages of a high specific surface area and filling density [6]. However, the preparation process of this membrane is complex, and the mechanical strength is poor, so it is not suitable for high-pressure separation [18]. Yonge et al. [91] suggested that the increase of ionic strength of influent would increase the solute flux of hollow fiber membrane. Therefore, LBL method is often used in fabricating hollow fiber membrane. Emonds et al. [90] proposed a new manufacturing method. The spinneret technology was used in this method, which combined with ionic crosslinking, amino covalent crosslinking, and phase transformation [90]. The membrane has a low MWCO value of 280 Da [90]. The rejection rates of methanol and hexane of acid-doped PBI hollow fiber membrane are more than 98%, which is suitable for the food and pharmaceutical industry [37]. Figure 3 is a brief summary of NF preparation.

Properties of NF Membranes

Surface Charge

In most cases, NF membranes are negatively charged under neutral or alkaline conditions and positively charged under highly acidic conditions [6]. The charge on the surface of NF membrane is beneficial to the selective interception of multivalent ions [30]. Most commercial NF membranes are negatively charged due to the negative fixed charge on the polymer backbone such as sulfonic acid and carboxylic acid [8]. The positively charged NF membrane can be used to separate cations because of its positive surface. For example, with the increasing cost of lithium, lithium recovery has attracted the attention of researchers [92]. In the separation of Li^+ and Mg^{2+}, negatively charged NF membranes are less effective than positively charged NF membranes. The reason is that the negative surface of the negatively charged NF membrane is not conducive to the rejection of Mg^{2+} [93]. Compared with the negatively charged NF membrane (NF90), the positively charged NF membrane based on PES has improved salt removal rate ($MgCl_2$), pure water flux, and stability [93]. The removal rates of Zn, Mg, Cd, Cu, Ca, Ni, and Pb by PES NF membrane grafted with ED and MWCNT (ED-g- MWCNT) were over 90% [9]. This may be due to the Donnan effect of the positively charged

Table 4 Nanofillers used in NF fabrication

Membrane preparation method	Main materials	Substrate materials	Nanofiller	Solute	Pressure (bar)	Removal rate (%)	Flux recovery (%)	Pure water permeability ($Lm^{-2}\ h^{-1}\ bar^{-1}$)	References
Interfacial polymerization	MPD, TMC	PA	ZIF-93	Sunset yellow (450 $gmol^{-1}$)	8	90		0.24 ± 0.09	[48]
Interfacial polymerization	MPD, TMC	PI	ODA functionalized rGO	Sunset yellow (452 $gmol^{-1}$), Rose Bengal (1017 $gmol^{-1}$)		98.6, 98.1			[52]
Interfacial polymerization	PIP, TMC	PSF	Silica spheres	Na_2SO_4, NaCl	6	98, 44		9.85	[33]
Interfacial polymerization	PIP, TMC	PA	BNNTs	$MgSO_4$, $CaCl_2$, NaCl	3	90, 82, 40	95	4.5	[51]
Interfacial polymerization	PIP, TMC	PSF	Copper benzene-1,3,5-tricarboxylate (CuBTC)	$MgSO_4$, NaCl	6	97.31, 36.2		5.17	[84]
Interfacial polymerization	PIP, TMC	PES	GO-TETA	NaCl, Na_2SO_4	6	32.2, 65.3	95.3	12.2	[85]
Interfacial polymerization	M-phenylenediamine, TMC	Si_3N_4/ polyacrylonitrile	TiO_2@rGO	Bromothymol blue (624 $gmol^{-1}$), Rose Bengal (1017 $gmol^{-1}$)		95, 97			[54]
Interfacial polymerization	PEI, TMC	PES	Cellulose nanoparticles (CNCs)	$CuSO_4$, $CuCl_2$, PbC	4	98, 96.5, 90.8		5.98	[86]
Phase inversion		CA	Silver	Na_2SO_4, $MgSO_4$, NaCl, $MgCl_2$	5	96.4, 97.4, 83.5, 90.4		1.88	[69]
Phase inversion		PES	Fe_3O_4@SiO_2-NH_2	Cd (II), Methyl red (269.3 $gmol^{-1}$)	4	93 97	88	16.25	[66]
Phase inversion		PES	Periodic mesoporous organosilica	Pb (II), Na_2SO_4, $MgSO_4$, NaCl	4	93.1, 73, 41.6, 33.7	53.4	8.43	[87]
Phase inversion		PES	Polyvinyl alcohol-Fe_3O_4	Na_2SO_4	5.5	94	71.1	2.55	[88]
Phase inversion		PES	Fe_3O_4-polyvinylpyrrolidone	Na_2SO_4	5	77	89.5	1.98	[47]
Phase inversion		PES	Oleic acid-titanium oxide (OA-TiO_2)	Na_2SO_4, $Cu(NO_3)_2$	5	72, 60	56	3.64	[89]
Phase inversion	N-Methyl-2-pyrrolidone	PES	BNNS	Humic acid (1wt%, pH10)	8	95	Nearly 100	31	[50]

Table 4 (continued)

Membrane preparation method	Main materials	Substrate materials	Nanofiller	Solute	Pressure (bar)	Removal rate (%)	Flux recovery (%)	Pure water permeability ($Lm^{-2}\ h^{-1}\ bar^{-1}$)	References
Phase inversion		Polyvinyl chloride (PVC)	Triethylenetetramine modified multiwalled carbon nanotubes (TETA-MWCNTs)	Lanasol blue 3R (789.4 $gmol^{-1}$)	2	86.1	70.9	43	[78]
Layer-by-layer	Tannic acid	PES	ZIF-8	Na_2SO_4, NaCl	5	66.7, 29.7		5.1	[49]
Coating and firing		α-Al_2O_3	TiO_2-ZrO_2	Evans blue (960.79 $gmol^{-1}$), Acid red (635.59 $gmol^{-1}$)	3	100, 93		6.33	[75]
Vacuum filtration		Cellulose nitrate	Niobate nanosheet (NbN)-GO	Evans blue (960.8 $gmol^{-1}$), NaCl, Na_2SO_4	4	98 12.7, 59.9		20.2	[53]
Using slot-die coater	ethanol	PES	dGO	Methyl red (269 $gmol^{-1}$), Rose Bengal (1010 $gmol^{-1}$)	6	89.8, 63.9		30	[55]
		Nylon	rGO/GONR	Rose Bengal	5	99		312.8	[57]
		Polycarbonate	GO	Methylene blue (373.9 $gmol^{-1}$), Rose Bengal (1017.64 $gmol^{-1}$)	5	98, 85		26.9	[59]

Table 5 Synthesis of nanoparticles

Nanoparticles	Method of Synthesis	References
ZIF-93	Zinc nitrate hexahydrate $Zn(NO_3)_2{\cdot}6H_2O$ mixed with 4-methyl-5-imidazolecarboxaldehyde $C_5H_6N_2O$ and sodium formate NaCOOH	[48]
TA-ZIF-8	By layer by layer self-assembly, tannic acid TA-Zn^{2+} layer is synthesized on the substrate, and then adding Hmim	[49]
BNNS	Dispersing hexagonal boron nitride and sodium dodecyl sulfate by ultrasonic, microwave, and infrared	[50]
BNNTs	Synthesized from ammonia and boron powder, and Fe_2O_3 and MgO are added as catalyzers	[51]
TiO_2@rGO	TiO_2 is dispersed in organic solvent, microwave radiation is carried out after GO added	[54]
rGO/GONR	GO is reduced to rGO by hydrazine, and then the multiwalled carbon nanotubes are decompressed. Disperse rGO in multiwalled carbon nanotubes	[57]
dGO	The mixture of GO and NaOH is cut and ultrasonically dispersed	[55]
ODA functionalized rGO	ODA solution is added to GO suspension and stirred	[52]
GO	Hummers' method. The graphite is dissolved in sulfuric acid, and potassium permanganate and hydrogen peroxide are added	[59]
Silica spheres	Stober method	[33]
CNCs	CNCs can be purchased directly from the manufacturer and need ultrasonic dispersion before use	[86]
Silver	Add sodium borohydride into silver nitrate	[69]
Fe_3O_4@SiO_2-NH_2	Disperse Fe_3O_4 into deionized water, add sodium silicate solution, nitrogen, and n-hexane	[66]
Periodic mesoporous organosilica	Polyethylene oxide–polypropylene oxide–polyethylene is dripped into bis (triethoxysilyl) ethane. Aging in autoclave and collection of white precipitates	[87]
Polyvinyl alcohol- Fe_3O_4	Fe_3O_4 is added to polyvinyl alcohol and dispersed by ultrasound	[88]
Fe_3O_4–polyvinylpyrrolidone	Fe_3O_4 is added to polyvinylpyrrolidone and dispersed by ultrasound	[47]
Copper benzene-1,3,5-tricarboxylate (CuBTC)	Purchased from manufacturer, dissolved in polymer solution	[84]
Oleic acid-titanium oxide (OA-TiO_2)	TiO_2 nanoparticles are added to the mixture of oleic acid and n-hexane, filtered, and dried	[89]
Triethylenetetramine-modified multiwalled carbon nanotubes (TETA-MWCNTs)	MWCNTs are placed in a mixture of sulfuric acid and nitric acid in an ultrasonic bath. After that, it is refluxed in thionyl chloride, dimethyl formamide, and reacted with triethylene tetramine	[78]
GO-TETA	GO and TETA are ultrasonically dispersed in ethanol and dried under vacuum	[85]
TiO_2-ZrO	Propanol, TiTP, and ZrTB are mixed, then add 1-propanediol, H_2O, and hydrochloric acid	[75]
Niobate nanosheet (NbN)-GO	NbN is synthesized by niobium and triethanolamine, and NbN-GO is assembled by vacuum filtration	[53]

film and the interaction of amine residues on the surface of ED-g-MWCNT with heavy metals [9].

Permeability and Selectivity

There is a "trade-off" effect between the permeability and selectivity on NF membrane. Tang et al. [94] suggested that nanostructures on the membrane surface can effectively improve the permeability of the membrane while maintaining stable selectivity. Nanostructures depend on external stimuli to change the diffusion rate of aqueous monomers, including adding inhibitors to the aqueous phase or precisely adjusting the hydrophilicity of the matrix [94]. Hydrophilicity can improve the rejection rate, permeation flux, and antifouling ability of membrane [95]. Supramolecular chemistry can affect the space size of monomers through host–guest interaction, thus changing their diffusion rate [94]. The selectivity of NF membrane can be regulated by changing the surface charge. When the membrane is charged, the ions are retained, while, when the membrane is shielded, the ions pass through the membrane [96]. Deposition of metal oxide layer is a method to change the surface charge of NF membrane. The surface charge of metal oxides depends on the pH of aqueous solution [97]. Metal oxide layer is due to atomic and molecular layer deposition (ALD or MLD) [97]. Alucone is a kind of MLD, which is suitable

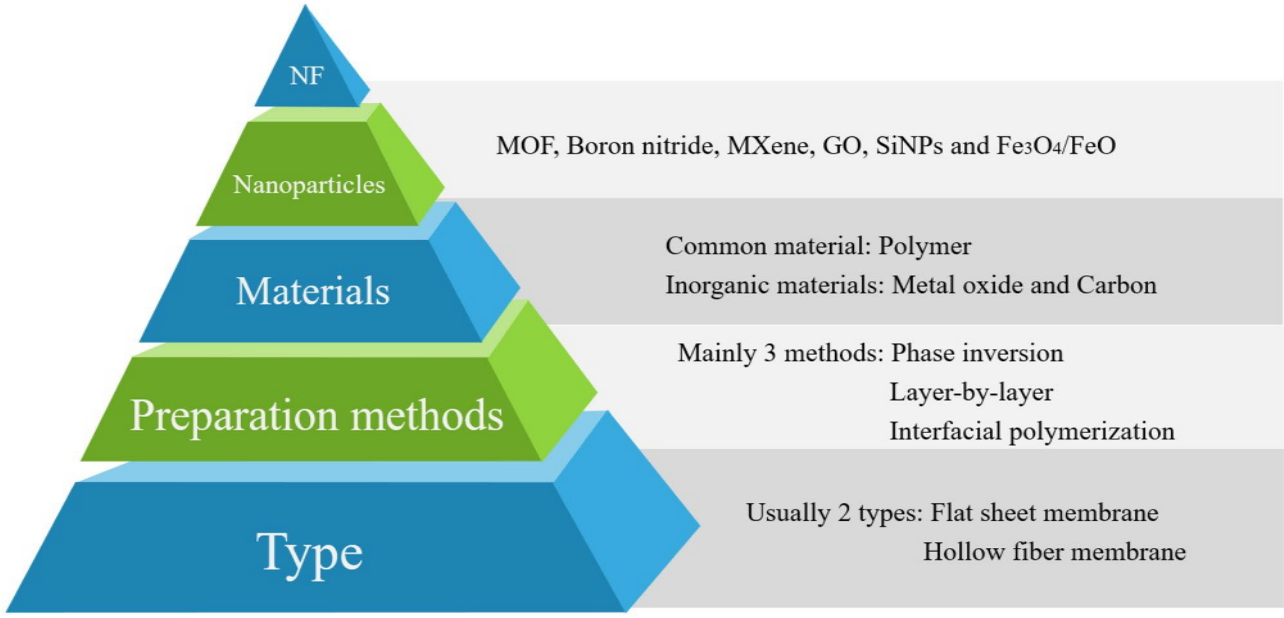

Fig. 3 A brief summary of NF preparation

for polymeric membrane. The permeability of NF membrane modified by alucone had little change, but the rejection rate increased [97]. This is due to the surface charge regulation of the active layer by alucone [97].

Morphology

Attenuated total reflectance-Fourier transform infrared spectroscopy (ATR-FTIR) is used to analyze the functional groups of the membrane [6]. Before using FTIR, the membrane needs to be dried to avoid the influence of atmospheric humidity [20]. Table 6 lists some characteristic peaks for identifying functional groups.

Hydrophilicity

The water contact angle is used to indicate the hydrophilicity of the membrane [35]. The smaller the water contact angle, the higher the hydrophilicity. Enhancing the hydrophilicity of membrane can improve the permeability and antifouling performance of the membrane. After adding carboxylated GO, the rejection rate of $MgSO_4$ by PSF NF membrane was 99.2% and the flux recovery was 92% [98]. Compared with the initial membrane, the rejection rate and flux recovery increased by 9.6% and 8%, respectively. Heidari et al. [99] synthesized carboxyl polyethersulfone membrane by acetylation and oxidation of PES. Compared with ordinary PES membrane, the water contact of synthetic membrane was reduced by 34°, and the flux recovery was increased from 59 to 86% [99]. This is because the hydrophilicity of the membrane surface reduces the hydrophobic force between surface and molecules to be separated.

Membrane Fouling

NF membrane fouling can be divided into organic, inorganic, and biological fouling. Although in research, the characteristics of each type of fouling are often analyzed independently, in practical applications, membrane fouling is caused by the three types of fouling simultaneously [100]. The formation of membrane fouling is affected by membrane materials, solutes, and operating parameters [100]. At the molecular level, the interaction between membrane surface and solute is mainly reflected in van der Waals force, chemical binding, and Lewis acid–base interaction [100]. Operating parameters, such as pH, affect protein solubility [100]. Besides the isoelectric point, the solubility of protein increases with the change of pH, thus affecting the flux [100]. Other operating parameters affecting membrane fouling include turbulence of feed flow, applied pressure, feed concentration, and temperature of the feed [100]. Unlike concentration polarization, membrane fouling is an irreversible process [101]. In this process, the membrane pores will be blocked, and the flux will continue to decrease, which can only be recovered by cleaning [100]. The behavior of membrane flux is usually described by a resistance-in-series model [100, 101]:

$$R_T = R_m + R_a + R_P + R_G + R_{cp} \tag{1}$$

$$J = \frac{\Delta P}{\eta R_T} \tag{2}$$

Table 6 Some characteristic peaks for identifying functional groups

Organic category	Characteristic peak (cm^{-1})	Corresponding functional group	References
Alkane	2960 and 2875	-CH_3 asymmetric and symmetric group stretching	[175]
	1460 and 1375	-CH_3 asymmetric and symmetric bending vibration	
	2925 and 2855	-CH_2 asymmetric and symmetric group stretching	
	1465	-CH_2 bending vibration	
	720 (Carbon > 4)	In plane rocking vibration	
Alkene	1680-1600	C=C	
	3100-3000	Stretching vibration of C-H bond adjacent to double bond <3000 C-H saturated >3000 C-H unsaturated	
	910 and 990	-C=C-CH_2 bending vibration	
	965 and 700	-R_1HC=CHR_2 (trans and formal configuration)	
Alkyne	2260-2100	C≡C	
	330 and 700-610	Stretching and bending vibration of C-H bond adjacent to triple bond	
Aromatic (Pictured is benzene) 	1600, 1500 and 1450	Benzene ring	
	3100-3000 900-650	=C-H stretching and bending vibration in benzene ring	
Alcohol and phenol (Pictured is phenol) 	3650-3590	-OH stretching vibration	
	1500-1250	-OH bending vibration	
	750-650	-OH rocking vibration	
	1300-1050	C-OH stretching vibration	
Ether 	1150-1050	C-O-C asymmetric stretching vibration	
Amine 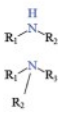	3500-3300	N-H stretching vibration	
	3300 and 3400	-NH_2 symmetric and asymmetric stretching vibration	
	1650-1500 and 950-600	-NH_2 in plane and out of plane bending vibration	
Ketone 	1715	C=O stretching vibration	
Aldehyde 	1725	C=O stretching vibration	
	2820 and 2720	C-H stretching vibration and bending vibration	
Carboxylic acid 	3300-3000	-OH stretching vibration	
	1725-1700	C=O stretching vibration	
	1350-1180	C-O stretching vibration	
Ester 	1756-1730	C=O stretching vibration	
	1300-1000	C-O stretching vibration	
Amide 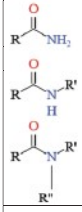	1680-1630	C=O stretching vibration	
	1570-1510	Coupling effect of N-H bending vibration and C-N stretching vibration	
	1335-1200	C-N stretching vibration	
	700	N-H bending vibration	
Acid anhydride 	1840-1820 and 1770-1740	C=O stretching vibration	
	1200-1000	C-O stretching vibration	

where, R_T is the total mass transfer resistance, R_m is membrane transport resistance, R_a is resistance due to adsorption of solutes onto membrane, R_P is resistance caused by membrane pore blockage, R_G is resistance produced by gel layer, R_{cp} is resistance produced by concentration polarization (both R_G and R_{cp} on the outer surface of the membrane facing the feed solution), J is permeate flux, ΔP is transmembrane pressure difference, and η is feed solution viscosity [100, 101].

Organic Fouling

Due to the organic pollutants (i.e., natural organic matter and polysaccharide) in water sources, NF membrane is vulnerable to organic fouling [102]. Organic fouling refers to the reduction of membrane flux caused by organic matter adsorbed onto the membrane surface to form a gel or deposited on the membrane pores [101]. The formation mechanism is related to the organic type, chemical properties, and the interaction with membrane materials [101]. Organic matter plays an important role in the process of the formation of foulants. The influence of organic matter can be divided into three kinds, they are the following: (a) adsorbed or deposited on the surface of membrane to cause fouling, (b) adsorbed on colloidal particles, (c) provided nutrition for microorganisms to accelerate biological fouling [101]. In the laboratory, SA is generally used to simulate organic pollutants [102, 103]. The decrease of permeate flux is due to the increase of hydraulic resistance of water flow and the prevention of salt back diffusion from membrane surface [102]. This phenomenon is called cake-enhanced concentration polarization (CECP) [102]. CECP usually leads to the increase of salt concentration on the membrane surface, resulting in the decrease of water driving force and flux [102]. In the process of cross flow membrane operation, the feed solution is concentrated along the feed channel due to the increase of permeation flux [104]. The discharged solute accumulated on and near the membrane surface, resulting in the increase of solute concentration in the whole feed channel [104]. Therefore, the concentration polarization layer is usually located in the feed channel. Thus, in practical applications, the concentration polarization near the outlet of membrane module is serious [104]. The existence of Ca^{2+} aggravates the membrane fouling because Ca^{2+} reacts with the carboxyl functional group of SA to form a SA fouling layer [102]. Through the complexation of organic calcium, calcium reduces the electrostatic repulsion of membrane foulants and increases the affinity of pollutants to the membrane surface, thus aggravating the organic fouling [102].

Inorganic Fouling

Inorganic fouling, also known as scaling, refers to the hard sediments formed in situ by inorganic substances [101]. Inorganic fouling can cause physical damage to the membrane [101]. Common fouling components are $CaCO_3$, $CaSO_4{\cdot}2H_2O$, silica, $BaSO_4$, $SrSO_4$, $Ca_3(PO_4)_2$, $Fe(OH)_3$, and $Al(OH)_3$ [101]. Inorganic foulants can form a filter cake or block the surface to reduce the flux, which involves nucleation and crystal growth [101]. The formation of a filter cake is due to the formation of porous layer on the surface of the membrane, the thickness of layer increases with time, and the lateral growth of crystal will block the surface [101]. As scale inhibitors can inhibit the nucleation rate, they are often used to reduce inorganic fouling [101].

Biological Fouling

Biological fouling refers to the fouling involving bioactive organisms [100]. Unlike passive deposition of organic and inorganic fouling, biological fouling is a dynamic process [100]. Microorganisms form colonies on the membrane surface and combine with glycocalyx in the colonies [101]. When the colonies grow to a certain extent, the membrane permeability decreases [100]. The way to alleviate the biological fouling is to destroy the glycocalyx, so that fungicides can enter the cells of biofilms [101]. Detergents or chelating agents are needed to destroy the glycocalyx. Oxidants are inefficient in this process, and some scale inhibitors provide growth substrates for microorganisms, so they are not recommended [101]. During chemical cleaning, the detergent should also be replaced in time to avoid microbial resistance.

Mitigation of Membrane Fouling

Membrane fouling will increase energy consumption and cleaning cost, reduce service life, and affect the competitiveness of the process [101]. Therefore, the mitigation of membrane fouling should not be ignored. This section will discuss how to alleviate membrane fouling from two aspects: pretreatment and cleaning methods.

Before using NF, it is necessary to avoid particles in the influent. MF and UF are often used as pretreatment of NF to remove particulate matter [101]. Activated carbon adsorption is a simple and effective pretreatment method. This method can effectively remove furan, phenols, and color from lignocellulosic biomass [105]. In addition, phenol and furan can be recovered while reducing NF fouling [105]. An advanced oxidation process can also be used as pretreatment of NF. For example, low doses of ferrous activated peroxymonosulfate can alleviate $CaSO_4{\cdot}2H_2O$ [106]. This may be due to the increase of interfacial free energy between membrane and fouling by adding ferrous activated peroxymonosulfate [106]. When electrodialysis is used as NF pretreatment, the ion content in feed can be reduced, thus reducing the possibility of fouling (Landsman et al. 2020).

NF membrane cleaning is usually divided into physical methods and chemical methods. Physical methods often use liquid turbulence to remove foulants, such as backwashing where water is pushed from the permeation side to the retention side [107]. The reverse flow discharges the dirt particles from the pores and loosens the dirt cake on the retention side [107]. Backwashing is not suitable for ceramic NF membrane because hydraulic shear force causes damage to the glass seal [103]. The chemical method is based on the repulsion between pollutant and membrane or reaction with pollutants [107]. Chemical cleaning damages the glass sealing layer of tubular ceramic NF membrane and destroys the environment when using sodium hypochlorite to remove organic pollutants [103]. Ultrasonic-assisted cleaning is an innovation of traditional physical cleaning method, which uses ultrasonic cavitation to generate vibration in liquid [107]. Ultrasound assistance generally operates at low frequencies to avoid damage to the membrane and can be used during operation [107]. The membrane flux recovery can reach 78% by this method, which is 20% higher than the backwash [107].

Theory and Modeling

The separation of NF membranes is controlled by 3 different mechanisms, namely steric hindrance (or size screening), Donnan effect (electrostatic), and dielectric exclusion [6]. Substances with a hydrated size larger than the membrane pore size are removed by steric hindrance, while the transport of species with a size similar to the membrane pores may be hindered [108]. In dielectric exclusion, the charged membrane repels ions with the same charge (co-ions) and attracts ions with opposite charge (counter ions) [108].

Separation Mechanism

Steric Hindrance Effect

The steric hindrance effect, or size screening, means that solutes larger than the pore size of the NF membrane may be rejected. NF is often used to separate sub nanometer-scale solutes, but the separation accuracy of steric hindrance effect is not accurate due to the uneven pore size of traditional TFC NF membrane [46]. A high pH increases the steric hindrance effect due to shrinkage of the membrane surface layer and reduction of the pore size [109]. High temperature reduces the steric hindrance effect due to the increase of the membrane

pore size and the increase of the compound diffusion coefficient [109].

Steric Hindrance Pore (SHP) Model

Nakao and Kimura (1982) proposed that the SHP model can be used to estimate the structural parameters of the membrane when the system is only composed of a single neutral solute [6, 110]. The model takes into account the effects of friction and steric hindrance on the transport of spherical ions through a cylindrical hole [110]. The membrane parameters σ and P_S can be calculated by SHP [6, 110]:

$$\sigma = 1 - S_F\left\{1 + \left(\frac{16}{9}\right)q^2\right\} \tag{3}$$

$$P_S = D \times S_D\left(\frac{A_k}{\Delta x}\right) \tag{4}$$

$$S_D = (1-q)^2 \tag{5}$$

$$S_F = 2(1-q)^2 - (1-q)^4 \tag{6}$$

$$q = \frac{r_s}{r_p} \tag{7}$$

where, P_S is the permeability coefficient of solute; σ is the reflection coefficient, that is, the quantitative index of real membrane deviates from ideal membrane; S_D and S_F are the solute distribution coefficients of diffusion and convection respectively [6, 110, 111]. D is the diffusion coefficient, $A_k/\Delta x$ is the ratio of membrane porosity to membrane thickness, r_s and r_p are Stokes radius of solute and membrane pore radius, respectively [110]. Stokes radius and diffusion coefficients of some ions are listed in Table 7. Using MATLAB R2020a to simulate the rejection rate of several ions in electrically neutral NF membrane, the results are shown in Fig. 4.

It can be seen from Fig. 4 that when NF is neutral, the rejection rate of ions is related to diffusion coefficient. The greater the diffusion coefficient, the lower the rejection rate. Assuming that the solutes are chloride and sodium ions, the thicknesses of the membrane selective layer are 20 μm and 40 μm; using MATLAB R2020a modeling, graphs of σ and P_S with respect to q can be obtained as shown in Fig. 5.

It can be seen from Fig. 5 that the value of P_S varies with different ions and is inversely proportional to the thickness of the selective layer. σ is dependent only to the ratio of solute radius to membrane pore radius, but not to the type of solute. Researchers found that pressurization and increasing the influent flow rate did not change σ significantly [112]. When σ is 0, the membrane is not selective and allows all solutes to pass through, but when σ is 1, the membrane will repel all solutes [111]. Normally, the larger the value of σ, the better the selectivity of the membrane to solutes. It can also be found from Fig. 4 that in using σ to describe the selectivity of membrane to solute, if the pore size of membrane remains unchanged, the larger the solute radius, the higher the value of σ, causing the higher selectivity. This is consistent with the phenomenon described in the literature. Researchers found that when using the same membrane, the rejection rate of NaCl is lower than that of $MgCl_2$ because σ of $MgCl_2$ is higher than that of NaCl [111].

Donnan Effect

Donnan effect or electrostatic repulsion is the expression of electrostatic force between solute and surface charge of polymer membrane, which mainly affects the separation of charged substances [113]. Based on Donnan effect, the selectivity of the membrane can be changed by controlling the electrostatic interaction. This is because the dissociation constant (pKa) of different compounds changes the surface charge of the system at different pH values [109]. In other words, the selectivity of the membrane to certain ions can be changed by adjusting the surface charge of the membrane [46]. For example, in the process of drug treatment, the removal rate of sulfamethoxazole is low because of its neutral charge [109]. However, carbamazepine has a high rejection rate because of its negative charge [109]. Similarly, the rejection rate of negative charged NF membrane for sulfate ion is higher than that for chloride ion, which is also due to co-ion with high valence is easily repelled [114]. Although the Donnan effect between the charged membrane and the co-ion provides the ability of ion repulsion, the electrostatic attraction between the membrane and the counter ion increases the fouling tendency of the membrane [30]. The development of Janus membrane may be an effective way to solve this problem.

If the two ions have the same net charge and similar hydration radius, the selectivity of the membrane to the two ions cannot be explained [108]. For example, Cl^- is more easily rejected by NF membrane than NO_3^- [108]. Some researchers think that this is due to the different hydration energy of ions, which depends on the charge and size of ions [108]. For example, Sigurdardottir et al. [115] considered

Table 7 Stokes radius and diffusion coefficients of some ions

Ion/solute	Na^+	Mg^{2+}	Ca^{2+}	Cl^-	SO_4^{2-}
D (10^{-9} m^2/s)	1.33	0.706	0.792	2.03	1.06
r_s (nm)	0.184	0.347	0.309	0.121	0.230

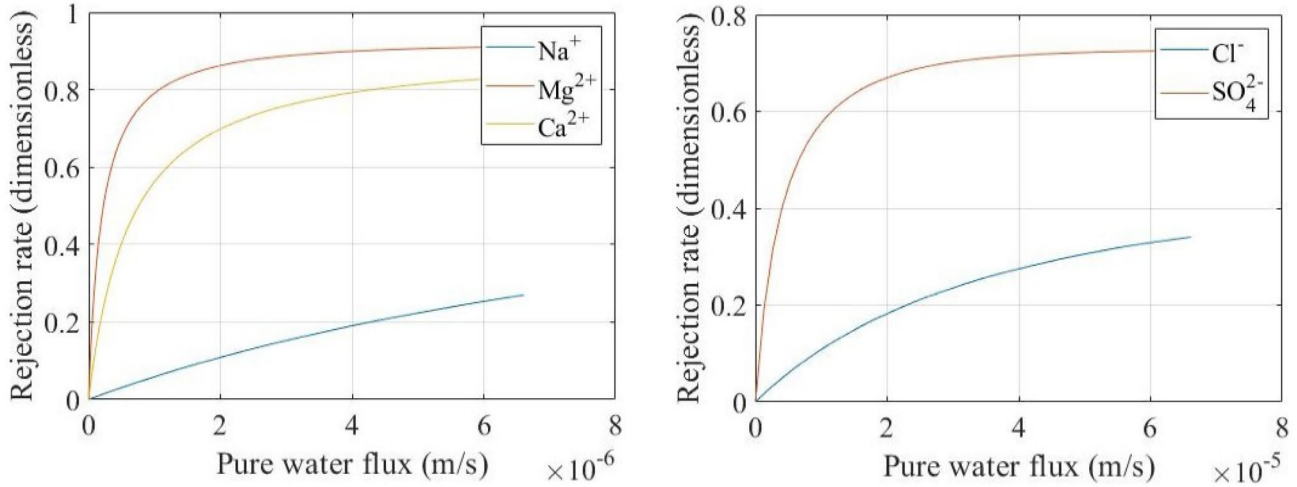

Fig. 4 Rejection rate of Na^+, Mg^{2+}, Ca^{2+}, Cl^-, and SO_4^{2-} in electrically neutral NF membrane

that higher hydration energy means higher energy required for ion dehydration, while the demand for ion dehydration increases with the decrease of pore size. When the hydration size of ions is similar to the membrane pore size, the higher hydration energy enhances the spatial repulsion of ions because the water shell around ions is not easy to remove or distort when passing through the membrane pore [115].

Still, the repulsion of F^- and Cl^- could not be explained [108]. F^- has a smaller ionic radius, a larger hydration size, and a higher hydration energy; and therefore, the NF membrane should have higher rejection of F^- than Cl^-, but the fact is the opposite [108]. Epsztein et al. [108] suggested that anions with small ionic radius (F^-) have a higher charge density than anions with a large ionic radius (Cl^-), so they are more susceptible to Donnan effect. Table 8 summarizes the rejection order of NF membrane in general.

Donnan-Steric-Pore Model (DSPM)

Bowen and Mukhtar developed the DSPM in 1996 [6]. DSPM is based on diffusion, convection, and electromigration, and takes ion migration into account [117]. DSPM

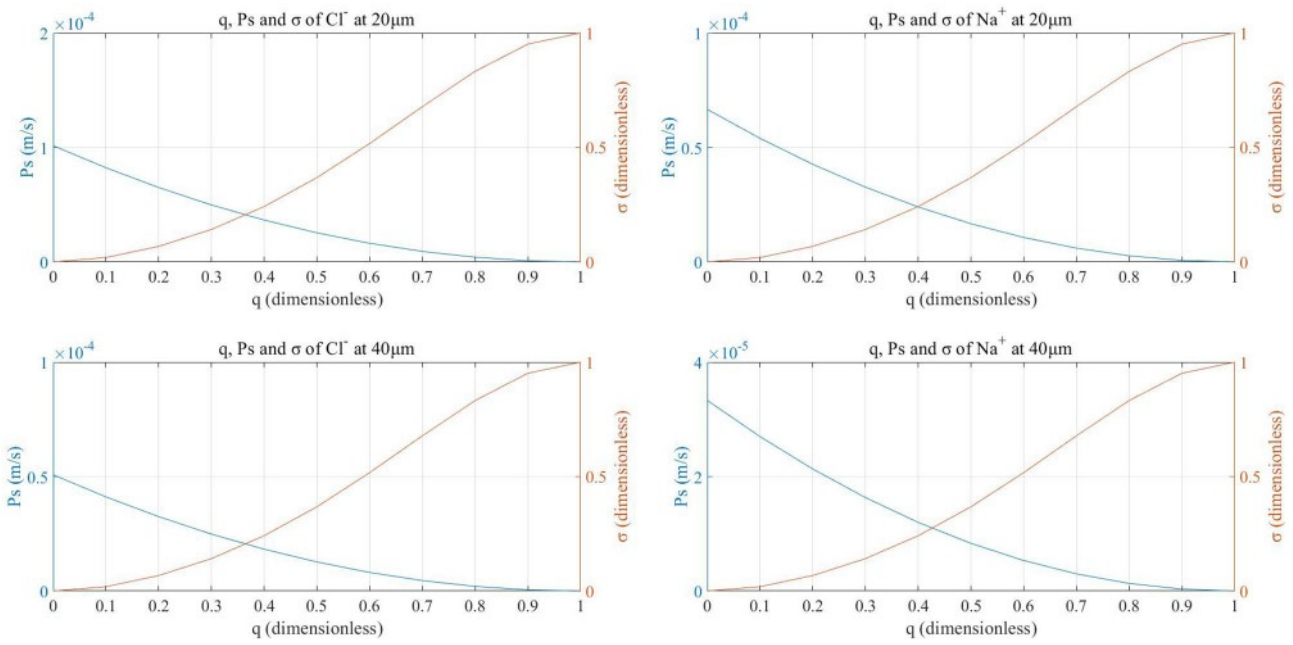

Fig. 5 Reflection coefficient, σ, and permeability coefficient, P_S, of solutes Cl^- and Na^+ with respect to the ratio of Stokes radius of the solutes and membrane pore radius, q

Table 8 NF membrane rejection order in general

Membrane type	Rejection order	Dominant separation mechanism	Reason for the separation	Commercial membranes	References
Positively charged NF	$CaCl_2 > NaCl > Na_2SO_4$	Donnan effect	The positively charged surface rejects Ca^{2+} and attracts SO_4^{2-}	MPF21, MPF32	[8, 116]
Negatively charged NF	$Na_2SO_4 > NaCl > CaCl_2$	Donnan effect	The negatively charged surface rejects SO_4^{2-} and attracts Ca^{2+}	ASP35, UTC70, HG01, HG19, BQ01, WFN0505	
Electrical neutral NF	$Na_2SO_4 > CaCl_2 > NaCl$	Steric hindrance	Diffusion coefficient: $NaCl > CaCl_2 > Na_2SO_4$	NF45, TFCS, CTA-LP, UTC90, SX10, MX07, CA30	

is derived from the extended Nemst-Planck equation and describes the diffusion and migration of ions on the membrane, which is due to the concentration and potential gradient as well as the convection caused by the pressure difference on the membrane [6, 117]. DSPM equation is shown below [6]:

$$J_i = -K_{i,d}D_i\frac{dc_i}{d_x} + K_{i,c}c_{i,0}J_j - \frac{z_i c_{i,0}K_{i,d}D_i}{RT}F\frac{d\varphi}{dx} \quad (8)$$

where J_i and J_j are solute and solvent fluxes respectively, and $K_{i,d}$ and $K_{i,c}$ are obstructing factors of diffusion and convection, respectively, and given by

$$K_{i,c} = \left(2-\theta_i\right)\left(1+0.054\lambda_i - 0.988\lambda_i^2 + 0.441\lambda_i^3\right) \quad (9)$$

$$K_{i,d} = 1 - 2.3\lambda_i + 1.154\lambda_i^2 + 0.224\lambda_i^3 \quad (10)$$

where, θ_i=[=$(1\text{-}\lambda_i)^2$] is a steric hindrance factor, λ[=r_i/r_p]$_i$ is the friction coefficient, r_i is solute radius, r_p is pore radius, D_i is solute diffusivity, $c_{i,0}$ is the concentration of solute on the membrane during feeding, R is the gas constant, T is the temperature of the feed, z_i is the ion valence, F is the Faraday constant, and dφ/dx is the potential gradient across the membrane [6, 117]. According to this equation, solute flux is affected by diffusion (driven by concentration gradient), convection (total volume flux), and Donnan effect [6]. For neutral solute applications, the last term on the right side of the Eq. (8) is negligible [6].

Researchers used DSPM to simulate the separation performance of commercial NF270. The results show that DSPM is accurate in simulating the separation performance of $NaSO_4$, and the average standard deviation is 2% [118]. Although DSPM is more accurate in predicting NF behavior, the calculation process is complex. To solve this problem, researchers developed a reduced order model (ROM) to simplify the DSPM calculation process. ROM can simplify the differential equation of DSPM into an algebraic equation [119]. However, concentration polarization must be considered when using ROM, otherwise the simulation results are inaccurate in the case of high concentration of feed [119].

Dielectric Exclusion (DE)

DE may interact with Donnan effect to regulate ion transport [46]. DE can be attributed to the change of dielectric constant of solvent from bulk to pore, which leads to solvation energy barrier and prevents the distribution of charged ions into pore (known as Born effect) [46]. Born effect explains the energy loss of hydration shell falling off when the ions move to the narrow channel in the pore, in which there is not enough space to accommodate all ions' hydration shell [120]. Unlike Donnan effect, DE is the repulsion of ions without considering the charge of ions [120]. Figure 6 is an explanation of steric hindrance, Donnan effect, and dielectric exclusion.

Donnan-Steric-Pore Model with Dielectric Exclusion (DSPM-DE)

Compared with the DSPM mentioned above, DSPM-DE adds the dielectric exclusion. The three rejection mechanisms are expressed as follows [120]:

$$\frac{\gamma_{i,pore}c_{i,pore}}{\gamma_{i,m}c_{i,m}} = \varphi_i\varphi_B exp\left(-\frac{z_iF}{RT}\varphi_{D,m}\right)|_{in} \quad (11)$$

where, $C_{i,\,pore}$ is the solute concentration at the entrance of the pore; $C_{i,\,m}$ is the feed concentration at the membrane feed solution interface; $\gamma_{i,\,m}$, $\gamma_{i,\,pore}$ are the activity coefficients of solute i at the membrane feed solution interface and at the entrance of the pore, respectively [120]. φ_i and φ_B are the spatial distribution factor and the Born fusion distribution factor, respectively [120]. φ_i and φ_B indicate the degree of rejection experienced by ions due to three effects, the smaller their value, the higher the extent of rejection [120]. If the values of φ_i and φ_B are small, the ratio of $C_{i,\,pore}$ to $C_{i,\,m}$ decreases [120]. $\varphi_{D,\,m}$ is the Donnan potential on the

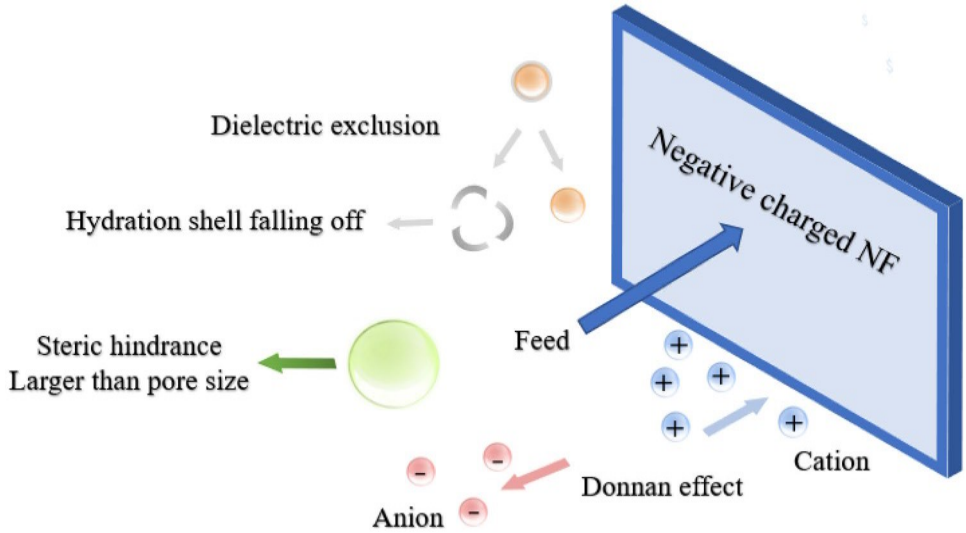

Fig. 6 Explanation of steric hindrance, Donnan effect, and dielectric exclusion

feed side, which means the potential difference between the solution at the entrance of the membrane pore and the interface of the feed film [120].

DSPM-DE model was used to simulate the NF performance of solutions containing Na^+, Cl^-, and Mg^{2+} in the literature. The results showed that the external pressure had little effect on the selectivity of the membrane when the concentration polarization was ignored [121]. However, the concentration of feed solute has a dominant effect on the selectivity, and the higher the concentration is, the worse the selectivity [121]. Wang and Lin [121] believed that this is due to the interaction of advection and electromigration in the DSPM-DE model. The higher the feed concentration, the lower the Donnan potential and the weaker the Donnan repulsion [121]. In the ternary system of Na^+, Cl^-, and Mg^{2+}, the selectivity of NF is less affected by the external pressure, but it is very sensitive to the feed concentration [121]. When SO_4^{2-} is present in the solution, NF membrane is negatively charged. The simulation results show that SO_4^{2-} has a higher repulsion rate than Cl^- due to its strong negative charge and enhances the repulsion rate of Na^+ and Mg^{2+} [121]. Improvement of Na^+ and Mg^{2+} rejection may be attributed to the neutral charge of the solution [121].

Characterization Method

Morphology of Membrane

The chemical structure of membrane is generally determined by ATR-FTIR [36]. The morphology of the membrane is characterized by scanning electron microscopy (SEM) and energy-dispersive X-ray spectroscopy (EDX) [41].

Zeta Potential

Ion exchange capacity is usually used to characterize the concentration of counter ions on NF membranes [8]. However, for NF membranes, the surface charge density is more important. The surface charge is usually quantified by measuring the streaming potential, which is the potential generated by the ion species flowing through the charged surface and can be converted into zeta potential (surface charge) [8]. The formation of electrostatic potential interacting with the ions present in the solution is related to the pH of the influent water and the concentration of the solution [122]. The streaming potential is measured by applying hydraulic pressure to force the electrolyte solution through the pore (vertical/flow) or across the surface of the membrane (tangential) [96].

Zeta potential is the potential difference between the smooth plane of the surface electric double layer (composed of the Stern layer and the diffusion layer) and the surrounding stable electrolyte [123]. Zeta potential represents the charge near the membrane, and is calculated by streaming potential (ζ) as follows [123]:

$$\zeta = \frac{dI}{dp} \times \frac{\eta}{\varepsilon_r \times \varepsilon_0} \times \frac{L}{A} \tag{12}$$

where, dI/dp is the flow current coefficient, L is the diaphragm length, A is the channel cross-sectional area, η is the viscosity, ε_0 is the vacuum permittivity, and ε_r is the relative permittivity of background solution [123].

Zeta potential can directly affect the membrane rejection rate. For example, when the ionic strength of brine is high and the zeta potential of the membrane is low, the rejection rate of sulfate decreases [123].

Membrane Hydrophilicity

The measurement of water contact angle needs a contact angle meter. Using the sessile drop method, the film sample is fixed on the slide, and then the image of a single droplet is recorded when the droplet is on the surface [124]. The contact angle can be obtained by analyzing the image. The water contact angle is calculated as follows [125]:

$$\cos\theta = \frac{\cos\theta_{app}}{r_W} \tag{13}$$

where, θ_{app} is the apparent contact angle and r_w is the ratio of the actual area of the surface to the projected area [125].

Porosity

The membrane porosity (ε%) is determined by gravimetric analysis, and the formula to calculate porosity is as follows [41, 126]:

$$\varepsilon = \frac{m_1 - m_2}{\rho_w A l} \tag{14}$$

where m_1 is the weight of the wet membrane film (g), m_2 is the weight of the dry film (g), A is the effective area of the film (cm^2), ρ_w is the water density (0.998 gcm^{-1}), and l is the film thickness (μm) [41].

Average Pore Diameter

The average pore size of the membrane can be estimated by Guerout-Elford-Ferry equation [47]:

$$r_m = \sqrt{\frac{(2.9 - 1.75\varepsilon)8\eta LQ}{\varepsilon A \Delta p}} \tag{15}$$

where, η, Q, ΔP, L, A, and ε are water viscosity (8.9×10^{-4} Pas), water permeate flow rate (m^3/s), operating pressure (0.45 MPa), membrane thickness (m), membrane area (m^2), and porosity, respectively [47].

Membrane Permeability

The permeability of membrane is usually calculated by the following formula [36]:

$$Permeability = \frac{m}{\rho \times A \times t \times P} \tag{16}$$

where m (kg) is the mass of permeate collected after a certain time t (h), P (MPa) is the applied pressure, A (m^2) is the effective area of membrane, and ρ is the water density (1 kg/L) [36].

Membrane Flux Recovery

Membrane flux recovery is calculated by the following formula [50]:

$$FR(\%) = \frac{J_{AF}}{J_{BF}} \times 100 \tag{17}$$

where, J_{BF} and J_{AF} are the pure water fluxes before and after membrane fouling and cleaning, respectively [50].

Transmission Model

There are generally three mechanisms for solute transport in NF membranes: diffusion (based on concentration gradient), convection (based on transmembrane pressure difference), and electromigration [113].

Hagen-Poiseuille Equation

Darcy's law gives the volume flow rate per unit area through porous material J_v, which is proportional to the pressure gradient, $J_v = K(\Delta P/l_m)$, K is Darcy's constant, ΔP is pressure drop, and l_m is membrane thickness [127]. When applied to asymmetric membranes, l_m is the thickness of the active layer [127]. If the viscosity η is introduced into the equation, then [6, 127]:

$$J_V = \frac{k}{\eta}\frac{\Delta p}{l_m} \tag{18}$$

where, k is a constant ($k = K\eta$), which depends only on the geometric properties of the porous membrane [6, 127].

Assuming that the membrane consists of a bunch of cylindrical holes perpendicular to the two membrane surfaces, the Navier–Stokes equation can be solved by using the wall slip free condition and the incompressible steady flow, the flux Hagen-Poiseuille equation can be obtained [6, 113, 127]:

$$J_V = \frac{\pi n_p \Delta p}{8\eta l_m} r_p^4 = \frac{\varepsilon \Delta p}{8\eta l_m} r_p^2 \tag{19}$$

where, n_p is the number of pores per unit area, and ε is the surface porosity [6, 113, 127].

Rejection rate of a solute is usually expressed as [113]:

$$R_S = 1 - \frac{C_{S,P}}{C_{S,R}} \tag{20}$$

where, R_s represents the rejection rate; $C_{S,P}$ and $C_{S,R}$ represent the solute concentrations in permeate and retention respectively [113].

For uncharged molecules, the Donnan effect has little influence, and the transmission is mainly affected by diffusion and convection. The uncharged solute transmission

model is usually expressed by the following formula, which takes into account the diffusion and convection terms [113]:

$$J_s = K_{S,C} C_S J_V - \frac{C_S D_{S,p}}{R_g T}\left(\frac{d\mu_s}{d(x/\varepsilon)}\right) \quad (21)$$

where, J_s and J_v represent the solute and the total volume flux through the membrane, $K_{s,c}$ is the convective resistance coefficient, C_s is the solute concentration in the membrane pores, $D_{s,p}$ refers to the diffusion rate of the blocked solute in the pores, R is the gas constant, T stands for absolute temperature, μ represents the chemical potential of the substance, and x is the axial coordinate in the membrane pore, ε is the porosity [113].

Application of NF Membranes for Water Purification and Industrial Separation

Drinking Water Treatment

Selenium (Se) is highly soluble and toxic in water, so it is a difficult problem to treat selenium-polluted groundwater. China, Japan, Jordan, the USA, Ireland, and India are all affected by excessive selenium in groundwater [128]. Malhotra, Pal, and Pal [128] applied commercial PA NF membrane to groundwater treatment in the Punjab province of India. NF membrane can effectively remove selenium from groundwater with a rejection rate of 98% and high flux under low pressure [128]. Meanwhile, in the long-term operation (250 h), the membrane module had almost no fouling [128]. Arsenic (As) pollution in drinking water affects more than 230 million people worldwide [112, 129]. Under normal circumstances, As exists in the earth's crust, but it can pollute water bodies through natural or human factors. For example, in Bangladesh and Argentina, seawater intrusion caused by climate change leads to As pollution of groundwater [130]. Human factors include the use of As pesticides, gold mining, and coal-fired power generation [130]. The removal rate of As by commercial NF90 can reach 93%, which is less affected by water pH and has market competitiveness [130]. The rejection rate of As by commercial HL NF membrane can reach 98% [131]. If the influent is pre-oxidized, the rejection rate can be further improved [131]. Fluoride is a serious and common groundwater quality problem in Tanzania [132]. Bouhadjar et al. [132] applied commercial NF90 to groundwater treatment in Boma Ngombe, northern Tanzania. After NF treatment, the fluoride content in groundwater decreased significantly from 60 to 1.5 mg/L [132].

In surface water treatment field, when submerged flat sheet NF is directly used, the removal rate of color and organic matter is more than 80%, and the effluent quality is stable [133]. Hexafluoropropylene oxide dimer acid (HFPO-DA) can be used as a processing aid in the production of fluoropolymers [134]. HFPO-DA has been detected in surface water and drinking water of downstream production bases in China, the USA, and Europe, with a concentration of 4500 ng/L [134]. The removal rate of HFPO-DA by NF membrane can reach 99.5%, which can be applied to the remediation of water environment [134].

Wastewater Reuse

NF is also used in industrial wastewater treatment, for example, to remove Pb^{2+} and Cu^{2+} from heavy metal water [86]. India discharges 50,000 m^3 of leather wastewater every day, which contains a high content of heavy metals [135]. The combination of NF and forward osmosis can improve effluent quality and reduce membrane fouling [136, 137]. The combination provides a new solution to leather wastewater. Car washing wastewater consumes a large amount of fresh water. Due to the use of chemicals, the wastewater contains high concentration of grease, surfactant, wax, salt, dust, and metal [138]. Electrocoagulation can precipitate metal species by forming metal hydroxide [139]. The recycling of car washing wastewater can be realized by using electrocoagulation-NF process [138].

Key raw materials are the necessary foundation for the production of high-tech products, while only a few industrial countries have raw material reserves [140]. Due to supply dependence, various strategic elements (such as Ag, Co, Cu, Ge, Mo, Re, Sn, Zn) are closely related to the EU economy [141]. Meschke et al. [141] used 8 commercial NF membranes to recover flue dust from copper smelting in Germany. The retention rates of Co^{2+}, Cu^{2+}, and Zn^{2+} of the eight NF membranes were all above 97%, and the NF99HF membrane was suitable for the separation of Ge and Mo [141]. The acid mine water has high acidity (pH < 3), high content of H_2SO_4 and metal (aluminum, iron, copper, and zinc), and rare earth elements [142]. Generally, the acid flow contains 1–50 wt% H_2SO_4, and the contents of copper, zinc, and iron are up to 2.5 g/L, mercury 0.05 g/L, lead 0.05 g/L, and arsenic 10 g/L [143]. In traditional methods, acid and metal ions in wastewater are treated by neutralization and flocculation/precipitation, which can produce secondary pollutants as precipitates [144]. NF can concentrate metals and rare earth elements and recover sulfuric acid and at the same time can reduce the cost [142]. When commercial MPF-34 NF membrane was used to treat acid flow, the metal rejection rate was about 80%, and the metal rejection rate was not affected by the concentration of main metal ions in the wastewater [145].

Industrial Stream Separation

In the field of industrial production, the use of NF for wastewater treatment in a sulfuric acid production plant is

expected to reduce annual water consumption by 551,880 m^3 and annual cost savings of US$ 99,000 [146]. Canada's oil sands deposits are an important source of crude oil in the global market, with an output of about 1.5 million barrels per day [147]. The tailings flow of mining is composed of 44 wt% water, 1 wt% residual asphalt, and 55 wt% solids [147]. In 2 years of tailings flow treatment, the removal rates of total suspended solids (TSS) and total organic carbon (TOC) by titanium dioxide ceramic NF membrane were almost 100% and 75%, respectively [147].

In addition, NF membranes are also used in sugar recovery, textile industry, food processing, and other fields [26, 113, 148]. Textile industry is an emerging industry; wet processing consumes a lot of water and produces 17–20% of industrial wastewater [149]. At present, more than 100,000 kinds of commercial synthetic dyes are used in various industries [150]. When dyes are decomposed, naphthalene, benzidine, and other aromatic by-products may be formed [151]. More than 7×10^5 tons of dyes is produced and consumed in the world every year [150]. About 10–15% of the dyes are discharged into the water source as untreated wastewater [150]. Some dyes can cause damage to the human kidney, and liver, and digestive, reproductive, and central nervous systems [150]. NF can reduce the impact of dye wastewater on human body and environment. When the treatment capacity is 1000 m^3/day, the operation cost of NF for dye removal is 0.81 US$/$m^3$ [25]. When NF is combined with electrocoagulation, the color removal rate is increased by 8%, and the membrane fouling is alleviated [149]. Raw galacto-oligosacchares (GOS) are a mixture of oligosaccharide, unreacted lactose, and monosaccharide, which need to be purified in medicine and food industry [152]. Lactose prevents the use of GOS in lactose-intolerant food formulations, increases the caloric value of GOS, and reduces the ability of prebiotics, thus limiting the use of GOS in low-calorie food formulations for infants, diabetes, and low-calorie products [152]. Using TriSep XN45 NF membrane to purify GOS at 20 bar and 45 °C, the final purity of GOS was 72% and the recovery rate of GOS was 87% [152]. NF is also used to concentrate fructose and sucrose solutions [153]. The rejection rate of commercial NFX NF membrane to fructose is 97% [154]. In the extraction and purification of vegetable oil, NF may become a new generation of crude oil processing technology [155].

Emerging Micropollutant Treatment

NF can be used to treat emerging micropollutants (EMP), such as personal care products (PPCP), endocrine-disrupting compounds (EDC), and pharmaceuticals (PhACs) [46, 109]. Commercial TFC-PA NF membranes can be used for most EMP removal, but they cannot effectively separate EMP from inorganic ions [46]. Drug residues include active pharmaceutical ingredient (API), including antibiotics, hormones, analgesics, anti-inflammatory drugs, blockers, and cell inhibitors [156]. Some APIs cannot be effectively degraded, and the degradable APIs are transformed into products with a similar structure, which are harmful to the environment [156]. The rejection rate of commercial AFC80 NF membrane on API is more than 98% [156]. Atenolol (ATN) is an important class of cardiovascular drugs, which is widely used in the treatment of coronary artery disease, hypertension, and arrhythmia [157]. ATN cannot be completely biodegraded in water. ATN has been found in municipal wastewater treatment plants in South Korea, Spain, Greece, Czech Republic, Sweden, India, Portugal, and South Africa [158]. The retention of commercial NF33 membrane to ATN is $70.9 \pm 3.5\%$ at pH 9, and the cost is estimated to be 0.53 US$/$m^3$ [157]. The wastewater treatment plant in Medina-Sidonia, southwestern Spain, uses NF to remove antibiotics (amoxicillin and penicillin G) and stimulants (theobromine and theophylline), and the water quality meets all the purposes of water regeneration and reuse in Spanish Royal Ordinance 1620/2007 [159]. The results of DK NF membrane treatment of Brazil Doce River showed that DK membrane had a high rejection rate for hydrophilic PhACs [160]. Anticancer drugs can effectively kill fast-growing tumor cells, but due to the lack of selectivity, they can also attack healthy cells, causing cytotoxicity, genotoxicity, mutagenicity, and teratogenicity [161]. Therefore, anticancer drugs are at high risk for personal health, especially for children, pregnant women, and the elderly [161]. In the next 20 years, the annual cancer cases are expected to reach 22 million, which means that the consumption of anti-cancer drugs increases sharply [161]. Desal 5DK NF membrane showed high efficiency in the treatment of anticancer drugs in hospital wastewater [161]. The performance of NF membrane to PPCP is affected by temperature. When the temperature increases from 5 to 25 ℃, the pure water permeability of NF membrane increases obviously [162]. This may be due to the decrease of the ability of membrane to selectively remove multivalent ions with the increase of temperature [163].

Medical Treatment

In the medical field, NF can be used to treat acute viral hepatitis. Acute viral hepatitis caused by hepatitis E virus (HEV) is a kind of zoonosis, which is transmitted through plasma, red blood cells, and platelets [164]. NF can enhance the intermediates in the immunoglobulin process and help eliminate HEV through neutralization [164]. Small non-carrying parvovirus B19 is caused by some plasma products, which may lead to the decrease of erythrocyte survival rate and the impairment of immune function [165]. The results of real-time quantitative polymerase chain reaction showed that B19 virus particles could be

Table 9 A brief summary of NF applications

Fields of application	Cases
Drinking water treatment	Remove Se, As, fluoride, and HFPO-DA
Wastewater reuse	Remove Pb and Cu, treatment of leather and car washing wastewater, Recycle Co, Cu, Zn, Ge, and Mo
Industrial stream separation	Save the production cost of sulfuric acid, treat the tailings flow of mining plant, treatment of textile wastewater, and sugar purification
Emerging micropollutants treatment	Remove PPCP, EDC, and PhACs
Medical treatment	Treat acute viral hepatitis and remove B19 virus
Combination technology	Combined with RO, membrane distillation, membrane capacitance, and electrodialysis to improve performance

removed by NF [165]. NF can also remove pathogens from plasma-derived products, which can be attributed to steric effect [166].

Combination of Technologies

NF can also be used in combination with other treatment technologies. Commercial TFC-PA NF membrane can also be used as a post-treatment process after acid hydrolysis or wet oxidation to convert sludge into an inorganic phosphorus-rich liquid phase [46]. Ceramic NF membrane can be used to separate phosphate from municipal wastewater [167]. Vibratory shear enhanced processing (VSEP) technology is further improving the phosphorus recovery efficiency and minimizing the volume of NF concentrate [168]. NF is also commonly used as pretreatment to reduce mineral fouling in subsequent processes such as RO and membrane distillation, and to enhance separation performance [46]. For example, in the desalination process, in order to prevent the subsequent process fouling, carbon dioxide, magnesium, calcium, and sulfate are removed by stripping, precipitation, ion exchange, and NF [169]. Furfural is a kind of furan platform chemical instead of fossil fuel [170]. The combination of NF and RO provides a guarantee for the concentration of furfural [170]. The combination of NF and membrane distillation can effectively avoid silica scaling, and membrane distillation can maintain a stable high rejection rate (> 99.8%) [171]. NF and membrane capacitive deionization coupling have the characteristics of high efficiency and energy saving in desalination of brine [172]. Compared with other separation methods, the composite process of NF and electrodialysis has economic advantages in the production of magnesium-rich brine [173]. NF can be used to purify solutions with a high ionic strength (ion concentration more than 1 mol/L) [174]. Traditional treatment of natural organic matter (NOM) is ion exchange, but it may produce polluted reclaimed brine and increase the cost. However, using ceramic NF membrane, the rejection rate of NOM can still reach more than 97% even at a high ionic strength [123]. Table 9 is a brief summary of NF applications.

Conclusion

In recent years, NF has gradually come into attention in improving water environment. The preparation method and raw material selection of NF gradually tend to green and simplification. With the development of new materials and preparation methods, NF has a wider application space in water purification. However, due to the special and complex separation mechanism of NF, the selectivity of some ions is not clear, so the modeling cannot be accurate. In the literature, there are few reports on the separation mechanism. In the aspect of membrane modification, the addition of nanoparticles contributed to the improvement of NF performance. Nevertheless, this modification is generally limited to the improvement of the rejection rate of one or several ions. In practical applications, the composition of influent is complex, and it is rarely reported whether the modifications will affect other ions. In addition, membrane fouling is still a challenge limiting the application of NF. Therefore, further in-depth studies on NF separation, fouling, and cleaning mechanisms, as well as vigorously developing new materials for the synthesis of NF membranes, will contribute to the market influence of NF.

Compliance with Ethical Standards

Conflict of Interest On behalf of all authors, the corresponding author states that there is no conflict of interest.

Human and Animal Rights and Informed Consent This article does not contain any studies with human or animal subjects performed by any of the authors.

References

1. Hou C, Wen Y, Liu X, Dong M. Impacts of regional water shortage information disclosure on public acceptance of recycled

water—evidences from China's urban residents. J Clean Prod. 2021;278:123965.
2. Gil A, Galeano LA, Vicente MÃ. Applications of advanced oxidation processes (AOPs) in drinking water treatment. 1st ed. Cham: Springer International Publishing; 2019.
3. Pathak V, Ambrose RPK. Starch-based biodegradable hydrogel as seed coating for corn to improve early growth under water shortage. J Appl Polym Sci. 2020;137(14):48523.
4. Mall NK, Herman JD. Water shortage risks from perennial crop expansion in California's Central Valley. Environ Res Lett. 2019;14(10):104014.
5. Mulder M. Basic principles of membrane technology. 2nd ed. Dordrecht: Springer, Netherlands; 1996.
6. Jye LW, Ismail AF. Nanofiltration membranes: synthesis, characterization, and applications. Boca Raton: CRC Press Taylor & Francis Group; 2017.
7. Shin MG, Kwon SJ, Park H, Park Y-I, Lee J-H. High-performance and acid-resistant nanofiltration membranes prepared by solvent activation on polyamide reverse osmosis membranes. J Membr Sci. 2020;595:117590.
8. Kamcev J, Freeman BD. Nanofiltration membranes. In: Kobayashi S, Müllen K, editors. Encyclopedia of polymeric nanomaterials. Berlin: Springer, Berlin Heidelberg; 2014. p. 1–9. https://doi.org/10.1007/978-3-642-36199-9_160-1.
9. Peydayesh M, Mohammadi T, Nikouzad SK. A positively charged composite loose nanofiltration membrane for water purification from heavy metals. J Membr Sci. 2020;611:118205.
10. Abdullah N, Yusof N, Ismail AF, Lau WJ. Insights into metal-organic frameworks-integrated membranes for desalination process: a review. Desalination. 2021;500:114867.
11. Yang Z, Zhou Y, Feng Z, Rui X, Zhang T, Zhang Z. A review on reverse osmosis and nanofiltration membranes for water purification. Polymers. 2019;11(8):1252.
12. Konca K, Çulfaz-Emecen PZ. Effect of carboxylic acid crosslinking of cellulose membranes on nanofiltration performance in ethanol and dimethylsulfoxide. J Membr Sci. 2019;587:117175.
13. Pandey RP, Rasheed PA, Gomez T, Azam RS, Mahmoud KA. A fouling-resistant mixed-matrix nanofiltration membrane based on covalently cross-linked Ti3C2TX (MXene)/cellulose acetate. J Membr Sci. 2020;607:118139.
14. Nguyen Thi HY, Nguyen BTD, Kim JF. Sustainable fabrication of organic solvent nanofiltration membranes. Membranes. 2020;11(1):19.
15. Wang H, Jung JT, Kim JF, Kim S, Drioli E, Lee YM. A novel green solvent alternative for polymeric membrane preparation via nonsolvent-induced phase separation (NIPS). J Membr Sci. 2019;574:44–54.
16. Qiu Z, Ji X, He C. Fabrication of a loose nanofiltration candidate from polyacrylonitrile/graphene oxide hybrid membrane via thermally induced phase separation. J Hazard Mater. 2018;360:122–31.
17. Aburabie J, Emwas AH, Peinemann KV. Silane-crosslinked asymmetric polythiosemicarbazide membranes for organic solvent nanofiltration. Macromol Mater Eng. 2019;304(1):1800551.
18. Turken T, Sengur-Tasdemir R, Sayinli B, Urper-Bayram GM, Ates-Genceli E, Tarabara VV, Koyuncu I. Reinforced thin-film composite nanofiltration membranes: fabrication, characterization, and performance testing. J Appl Polym Sci. 2019;136(39):48001.
19. Guo D, Xiao Y, Li T, Zhou Q, Shen L, Li R, Xu Y, Lin H. Fabrication of high-performance composite nanofiltration membranes for dye wastewater treatment: mussel-inspired layer-by-layer self-assembly. J Colloid Interface Sci. 2020;560:273–83.
20. Agarwal P, Hefner RE, Ge S, Tomlinson I, Rao Y, Dikic T. Nanofiltration membranes from crosslinked Troger's base polymers of intrinsic microporosity (PIMs). J Membr Sci. 2020;595:117501.
21. DuChanois RM, Epsztein R, Trivedi JA, Elimelech M. Controlling pore structure of polyelectrolyte multilayer nanofiltration membranes by tuning polyelectrolyte-salt interactions. J Membr Sci. 2019;581:413–20.
22. Elshof MG, de Vos WM, de Grooth J, Benes NE. On the long-term pH stability of polyelectrolyte multilayer nanofiltration membranes. J Membr Sci. 2020;615:118532.
23. Kyriakou N, Merlet RB, Willott JD, Nijmeijer A, Winnubst L, Pizzoccaro-Zilamy M-A. New method toward a robust covalently attached cross-linked nanofiltration membrane. ACS Appl Mater Interfaces. 2020;12(42):47948–56.
24. Duong PHH, Daumann K, Hong P-Y, Ulbricht M, Nunes SP. Interfacial polymerization of zwitterionic building blocks for high-flux nanofiltration membranes. Langmuir. 2019;35(5):1284–93.
25. Gunawan FM, Mangindaan D, Khoiruddin K, Wenten IG. Nanofiltration membrane cross-linked by m-phenylenediamine for dye removal from textile wastewater. Polym Adv Technol. 2019;30(2):360–7.
26. Ormanci-Acar T, Tas CE, Keskin B, Ozbulut EBS, Turken T, Imer D, Tufekci N, Menceloglu YZ, Unal S, Koyuncu I. Thin-film composite nanofiltration membranes with high flux and dye rejection fabricated from disulfonated diamine monomer. J Membr Sci. 2020;608:118172.
27. Das SK, Manchanda P, Peinemann K-V. Solvent-resistant triazine-piperazine linked porous covalent organic polymer thin-film nanofiltration membrane. Sep Purif Technol. 2019;213:348–58.
28. Zhao Y, Zhang Z, Dai L, Zhang S. Preparation of a highly permeable nanofiltration membrane using a novel acyl chloride monomer with -PO(Cl)2 group. Desalination. 2018;431:56–65.
29. Shi M, Yan W, Dong C, Liu L, Xie S, Gao C. Solvent activation before heat-treatment for improving reverse osmosis membrane performance. J Membr Sci. 2020;595:117565.
30. Hoffman JR, Phillip WA. Dual-functional nanofiltration membranes exhibit multifaceted ion rejection and antifouling performance. ACS Appl Mater Interfaces. 2020;12(17):19944–54.
31. Dipaola M, Wodajo FM. 3D printing in orthopaedic surgery. St Louis: Elsevier; 2019.
32. Park S, Jeong YD, Lee JH, Kim J, Jeong K, Cho KH. 3D printed honeycomb-shaped feed channel spacer for membrane fouling mitigation in nanofiltration. J Membr Sci. 2021;620:118665.
33. Ang MBMY, Pereira JM, Trilles CA, Aquino RR, Huang S-H, Lee K-R, Lai J-Y. Performance and antifouling behavior of thin-film nanocomposite nanofiltration membranes with embedded silica spheres. Sep Purif Technol. 2019;210:521–9.
34. Morales-Cuevas JB, Pérez-Sicairos S, Lin SW, Salazar-Gastélum MI. Evaluation of a modified spray-applied interfacial polymerization method for preparation of nanofiltration membranes. J Appl Polym Sci. 2019;136(42):48129.
35. Polisetti V, Ray P. Thin film composite nanofiltration membranes with polystyrene sodium sulfonate–polypiperazinetrimesamide semi-interpenetrating polymer network active layer. J Appl Polym Sci. 2020;137(44):49351.
36. Ji Y-L, Ang MBMY, Huang S-H, Lu J-Y, Tsai S-J, De Guzman MR, Tsai H-A, Hu C-C, Lee K-R, Lai J-Y. Performance evaluation of nanofiltration polyamide membranes based from 3,3′-diaminobenzidine. Sep Purif Technol. 2019;211:170–8.
37. Asadi Tashvigh A, Chung T-S. Robust polybenzimidazole (PBI) hollow fiber membranes for organic solvent nanofiltration. J Membr Sci. 2019;572:580–7.
38. Davood Abadi Farahani MH, Chung T-S. A novel crosslinking technique towards the fabrication of high-flux polybenzimidazole (PBI) membranes for organic solvent nanofiltration (OSN). Sep Purif Technol. 2019;209:182–92.
39. Agboola O, Fayomi OSI, Sadiku R, Popoola P, Alaba PA, Adegbola AT. Polymers blends for the improvement of

nanofiltration membranes in wastewater treatment: a short review. Mater Today Proc. 2021;43:3365–8.
40. Ang MBMY, Tang C-L, De Guzman MR, Maganto HLC, Caparanga AR, Huang S-H, Tsai H-A, Hu C-C, Lee K-R, Lai J-Y. Improved performance of thin-film nanofiltration membranes fabricated with the intervention of surfactants having different structures for water treatment. Desalination. 2020;481:114352.
41. Mahdavi H, Mazinani N, Heidari AA. Poly(vinylidene fluoride) (PVDF)/PVDF-g-polyvinylpyrrolidone (PVP)/TiO2 mixed matrix nanofiltration membranes: preparation and characterization. Polym Int. 2020;69(12):1187–95.
42. Van Goethem C, Mertens M, Vankelecom IFJ. Crosslinked PVDF membranes for aqueous and extreme pH nanofiltration. J Membr Sci. 2019;572:489–95.
43. Van Goethem C, Magboo MM, Mertens M, Thijs M, Koeckelberghs G, Vankelecom IFJ. A scalable crosslinking method for PVDF-based nanofiltration membranes for use under extreme pH conditions. J Membr Sci. 2020;611:118274.
44. Aburabie JH, Puspasari T, Peinemann K-V. Alginate-based membranes: paving the way for green organic solvent nanofiltration. J Membr Sci. 2020;596:117615.
45. Tham HM, Chung T-S. One-step cross-linking and tannic acid modification of polyacrylonitrile hollow fibers for organic solvent nanofiltration. J Membr Sci. 2020;610:118294.
46. Zhao Y, Tong T, Wang X, Lin S, Reid EM, Chen Y. Differentiating solutes with precise nanofiltration for next generation environmental separations: a review. Environ Sci Technol. 2021;55(3):1359–76.
47. Hosseini SM, Afshari M, Fazlali AR, Koudzari Farahani S, Bandehali S, Van der Bruggen B, Bagheripour E. Mixed matrix PES-based nanofiltration membrane decorated by (Fe3O4–polyvinylpyrrolidone) composite nanoparticles with intensified antifouling and separation characteristics. Chem Eng Res Des. 2019;147:390–8.
48. Echaide-Górriz C, Zapata JA, Etxeberría-Benavides M, Téllez C, Coronas J. Polyamide/MOF bilayered thin film composite hollow fiber membranes with tuned MOF thickness for water nanofiltration. Sep Purif Technol. 2020;236:116265.
49. Xiao Y, Zhang W, Jiao Y, Xu Y, Lin H. Metal-phenolic network as precursor for fabrication of metal-organic framework (MOF) nanofiltration membrane for efficient desalination. J Membr Sci. 2021;624:119101.
50. Low Z-X, Ji J, Blumenstock D, Chew Y-M, Wolverson D, Mattia D. Fouling resistant 2D boron nitride nanosheet – PES nanofiltration membranes. J Membr Sci. 2018;563:949–56.
51. Casanova S, Liu T-Y, Chew Y-MJ, Livingston A, Mattia D. High flux thin-film nanocomposites with embedded boron nitride nanotubes for nanofiltration. J Membr Sci. 2020;597:117749.
52. Paseta L, Luque-Alled JM, Malankowska M, Navarro M, Gorgojo P, Coronas J, Téllez C. Functionalized graphene-based polyamide thin film nanocomposite membranes for organic solvent nanofiltration. Sep Purif Technol. 2020;247:116995.
53. Kunimatsu M, Nakagawa K, Yoshioka T, Shintani T, Yasui T, Kamio E, Tsang SCE, Li J, Matsuyama H. Design of niobate nanosheet-graphene oxide composite nanofiltration membranes with improved permeability. J Membr Sci. 2020;595:117598.
54. Abadikhah H, Kalali EN, Behzadi S, Khan SA, Xu X, Shabestari ME, Agathopoulos S. High flux thin film nanocomposite membrane incorporated with functionalized TiO2@reduced graphene oxide nanohybrids for organic solvent nanofiltration. Chem Eng Sci. 2019;204:99–109.
55. Kim JH, Choi Y, Kang J, Choi E, Choi SE, Kwon O, Kim DW. Scalable fabrication of deoxygenated graphene oxide nanofiltration membrane by continuous slot-die coating. J Membr Sci. 2020;612:118454.
56. Mahalingam DK, Wang S, Nunes SP. Stable graphene oxide cross-linked membranes for organic solvent nanofiltration. Ind Eng Chem Res. 2019;58(51):23106–13.
57. Cho KM, Lee H-J, Nam YT, Kim Y-J, Kim C, Kang KM, Ruiz Torres CA, Kim DW, Jung H-T. Ultrafast-selective nanofiltration of an hybrid membrane comprising laminated reduced graphene oxide/graphene oxide nanoribbons. ACS Appl Mater Interfaces. 2019;11(30):27004–10.
58. Mahalingam DK, Falca G, Upadhya L, Abou-Hamad E, Batra N, Wang S, Musteata V, da Costa PM, Nunes SP. Spray-coated graphene oxide hollow fibers for nanofiltration. J Membr Sci. 2020;606:118006.
59. Nam YT, Kim SJ, Kang KM, Jung W-B, Kim DW, Jung H-T. Enhanced nanofiltration performance of graphene-based membranes on wrinkled polymer supports. Carbon. 2019;148:370–7.
60. Alhumaidi MS, Arshad F, Aubry C, Ravaux F, McElhinney J, Hasan A, Zou L. Electrostatically coupled SiO2 nanoparticles/poly (L-DOPA) antifouling coating on a nanofiltration membrane. Nanotechnology. 2020;31(27):275602.
61. Ang MBMY, Trilles CA, De Guzman MR, Pereira JM, Aquino RR, Huang S-H, Hu C-C, Lee K-R, Lai J-Y. Improved performance of thin-film nanocomposite nanofiltration membranes as induced by embedded polydopamine-coated silica nanoparticles. Sep Purif Technol. 2019;224:113–20.
62. Malakian A, Husson SM. Understanding the roles of patterning and foulant chemistry on nanofiltration threshold flux. J Membr Sci. 2020;597:117746.
63. Priyadarshini A, Tay SW, Ng S, Hong L. Skinned carbonaceous composite membrane with pore channels bearing an anchored surfactant layer for nanofiltration. J Membr Sci. 2020;599:117714.
64. Ashraf MA, Wang J, Wu B, Cui P, Xu B, Li X. Enhancement in Li+/Mg2+ separation from salt lake brine with PDA–PEI composite nanofiltration membrane. J Appl Polym Sci. 2020;137(47):49549.
65. Bahamonde Soria R, Zhu J, Gonza I, Van der Bruggen B, Luis P. Effect of (TiO2: ZnO) ratio on the anti-fouling properties of bio-inspired nanofiltration membranes. Sep Purif Technol. 2020;251:117280.
66. Kamari S, Shahbazi A. Biocompatible Fe3O4@SiO2-NH2 nanocomposite as a green nanofiller embedded in PES–nanofiltration membrane matrix for salts, heavy metal ion and dye removal: long–term operation and reusability tests. Chemosphere (Oxford). 2020;243:125282.
67. Lakhotia SR, Mukhopadhyay M, Kumari P. Iron oxide (FeO) nanoparticles embedded thin-film nanocomposite nanofiltration (NF) membrane for water treatment. Sep Purif Technol. 2019;211:98–107.
68. Poolachira S, Velmurugan S. Exfoliated hydrotalcite–modified polyethersulfone-based nanofiltration membranes for removal of lead from aqueous solutions. Environ Sci Pollut Res Int. 2020;27(24):29725–36.
69. Beisl S, Monteiro S, Santos R, Figueiredo AS, Sánchez-Loredo MG, Lemos MA, Lemos F, Minhalma M, de Pinho MN. Synthesis and bactericide activity of nanofiltration composite membranes – cellulose acetate/silver nanoparticles and cellulose acetate/silver ion exchanged zeolites. Water Res. 2019;149:225–31.
70. Nidhi Maalige R, Aruchamy K, Mahto A, Sharma V, Deepika D, Mondal D, Nataraj SK. Low operating pressure nanofiltration membrane with functionalized natural nanoclay as antifouling and flux promoting agent. Chem Eng J. 2019;358:821–30.
71. Averina YM, Kurbatov AY, Sakharov DA, Subcheva EN. Development of nanofiltration ceramic membrane production technology. Glass Ceram. 2020;77(3–4):98–102.
72. Anisah S, Kanezashi M, Nagasawa H, Tsuru T. Al2O3 nanofiltration membranes fabricated from nanofiber sols: preparation, characterization, and performance. J Membr Sci. 2020;611:118401.

73. Amirilargani M, Yokota GN, Vermeij GH, Merlet RB, Delen G, Mandemaker LDB, Weckhuysen BM, Winnubst L, Nijmeijer A, de Smet LCPM, Sudhölter EJR. Melamine-based microporous organic framework thin films on an alumina membrane for high-flux organic solvent nanofiltration. Chemsuschem. 2020;13(1):136–40.
74. Anisah S, Kanezashi M, Nagasawa H. Tsuru T. Hydrothermal stability and permeation properties of TiO2-ZrO2 (5/5) nanofiltration membranes at high temperatures. Sep Purif Technol. 2019;212:1001–12.
75. Sada Y, Yoshioka T, Nakagawa K, Shintani T, Iesako R, Kamio E, Matsuyama H. Preparation and characterization of organic chelate ligand (OCL)-templated TiO2–ZrO2 nanofiltration membranes. J Membr Sci. 2019;591:117304.
76. Qin H, Guo W, Huang X, Gao P, Xiao H. Preparation of yttria-stabilized ZrO2 nanofiltration membrane by reverse micelles-mediated sol-gel process and its application in pesticide wastewater treatment. J Eur Ceram Soc. 2020;40(1):145–54.
77. Chau J, Singh D, Sirkar KK. 110th anniversary: liquid separation membranes based on nanowire substrates for organic solvent nanofiltration and membrane distillation. Ind Eng Chem Res. 2019;58(31):14350–6.
78. Vatanpour V, Esmaeili M, Safarpour M, Ghadimi A, Adabi J. Synergistic effect of carboxylated-MWCNTs on the performance of acrylic acid UV-grafted polyamide nanofiltration membranes. React Funct Polym. 2019;134:74–84.
79. Manorma, Ferreira I, Alves P, Gil MH, Gando-Ferreira LM. Lignin separation from black liquor by mixed matrix polysulfone nanofiltration membrane filled with multiwalled carbon nanotubes. Sep Purif Technol. 2021;260:118231.
80. Zhang H, Quan X, Fan X, Yi G, Chen S, Yu H, Chen Y. Improving ion rejection of conductive nanofiltration membrane through electrically enhanced surface charge density. Environ Sci Technol. 2019;53(2):868–77.
81. Yang Y, Yang X, Liang L, Gao Y, Cheng H, Li X, Zou M, Ma R, Yuan Q, Duan X. Large-area graphene-nanomesh/carbon-nanotube hybrid membranes for ionic and molecular nanofiltration. Science. 2019;364(6445):1057–62.
82. Park MJ, Wang C, Seo DH, Gonzales RR, Matsuyama H, Shon HK. Inkjet printed single walled carbon nanotube as an interlayer for high performance thin film composite nanofiltration membrane. J Membr Sci. 2021;620:118901.
83. Rahimi Z, Zinatizadeh AA, Zinadini S, van Loosdrecht MCM. β-cyclodextrin functionalized MWCNTs as a promising antifouling agent in fabrication of composite nanofiltration membranes. Sep Purif Technol. 2020;247:116979.
84. Misdan N, Ramlee N, Hairom NHH, Ikhsan SNW, Yusof N, Lau WJ, Ismail AF, Nordin NAHM. CuBTC metal organic framework incorporation for enhancing separation and antifouling properties of nanofiltration membrane. Chem Eng Res Des. 2019;148:227–39.
85. Izadmehr N, Mansourpanah Y, Ulbricht M, Rahimpour A, Omidkhah MR. TETA-anchored graphene oxide enhanced polyamide thin film nanofiltration membrane for water purification performance and antifouling properties. J Environ Manag. 2020;276:111299.
86. Hoang MT, Pham TD, Verheyen D, Nguyen MK, Pham TT, Zhu J, Van der Bruggen B. Fabrication of thin film nanocomposite nanofiltration membrane incorporated with cellulose nanocrystals for removal of Cu(II) and Pb(II). Chem Eng Sci. 2020;228:115998.
87. Mehrjo F, Pourkhabbaz A, Shahbazi A. PMO synthesized and functionalized by p-phenylenediamine as new nanofiller in PES-nanofiltration membrane matrix for efficient treatment of organic dye heavy metal and salts from wastewater. Chemosphere. 2021;263:128088.
88. Bagheripour E, Moghadassi AR, Parvizian F, Hosseini SM, Van der Bruggen B. Tailoring the separation performance and fouling reduction of PES based nanofiltration membrane by using a PVA/Fe3O4 coating layer. Chem Eng Res Des. 2019;144:418–28.
89. Parvizian F, Ansari F, Bandehali S. Oleic acid-functionalized TiO2 nanoparticles for fabrication of PES-based nanofiltration membranes. Chem Eng Res Des. 2020;156:433–41.
90. Emonds S, Roth H, Wessling M. Chemistry in a spinneret – formation of hollow fiber membranes with a cross-linked polyelectrolyte separation layer. J Membr Sci. 2020;612:118325.
91. Yonge DT, Biscardi PG, Duranceau SJ. Modeling ionic strength effects on hollow-fiber nanofiltration membrane mass transfer. Membranes. 2018;8(3):37.
92. Park SH, Kim JH, Moon SJ, Jung JT, Wang HH, Ali A, Quist-Jensen CA, Macedonio F, Drioli E, Lee YM. Lithium recovery from artificial brine using energy-efficient membrane distillation and nanofiltration. J Membr Sci. 2020;598:117683.
93. Zhang Y, Wang L, Sun W, Hu Y, Tang H. Membrane technologies for Li+/Mg2+ separation from salt-lake brines and seawater: a comprehensive review. J Ind Eng Chem. 2020;81:7–23.
94. Tang M-J, Liu M-L, Wang D-A, Shao D-D, Wang H-J, Cui Z, Cao X-L, Sun S-P. Precisely patterned nanostrand surface of cucurbituril[n]-based nanofiltration membranes for effective alcohol–water condensation. Nano Lett. 2020;20(4):2717–23.
95. Urper-Bayram GM, Sayinli B, Sengur-Tasdemir R, Turken T, Pekgenc E, Gunes O, Ates-Genceli E, Tarabara VV, Koyuncu I. Nanocomposite hollow fiber nanofiltration membranes: fabrication, characterization, and pilot-scale evaluation for surface water treatment. J Appl Polym Sci. 2019;136(45):48205.
96. Árki P, Hecker C, Tomandl G, Joseph Y. Streaming potential properties of ceramic nanofiltration membranes – importance of surface charge on the ion rejection. Sep Purif Technol. 2019;212:660–9.
97. Chaudhury S, Wormser E, Harari Y, Edri E, Nir O. Tuning the ion-selectivity of thin-film composite nanofiltration membranes by molecular layer deposition of alucone. ACS Appl Mater Interfaces. 2020;12(47):53356–64.
98. Li H, Shi W, Du Q, Zhou R, Zhang H, Qin X. Improved separation and antifouling properties of thin-film composite nanofiltration membrane by the incorporation of cGO. Appl Surf Sci. 2017;407:260–75.
99. Heidari A, Abdollahi E, Mohammadi T, Asadi AA. Improving permeability, hydrophilicity and antifouling characteristic of PES hollow fiber UF membrane using carboxylic PES: a promising substrate to fabricate NF layer. Sep Purif Technol. 2021;270:118811.
100. Muhammad Akhyar F. Nanofiltration. IntechOpen; 2018.
101. Schäfer A, Andritsos N, Karabelas AJ, Hoek EMV, Schneider R, Nyström M. Fouling in nanofiltration. Edinburgh: Elsevier; 2004.
102. Mahlangu OT, Mamba BB, Verliefde ARD. Effect of multivalent cations on membrane-foulant and foulant-foulant interactions controlling fouling of nanofiltration membranes. Polym Adv Technol. 2020;31(11):2588–600.
103. Kramer FC, Shang R, Rietveld LC, Heijman SJG. Fouling control in ceramic nanofiltration membranes during municipal sewage treatment. Sep Purif Technol. 2020;237:116373.
104. Jung O, Saravia F, Wagner M, Heißler S, Horn H. Quantifying concentration polarization - Raman microspectroscopy for in-situ measurement in a flat sheet cross-flow nanofiltration membrane unit. Sci Rep. 2019;9(1):15885.
105. Li Y, Qi B, Wan Y. Separation of monosaccharides from pretreatment inhibitors by nanofiltration in lignocellulosic hydrolysate: fouling mitigation by activated carbon adsorption. Biomass Bioenergy. 2020;136:105527.
106. Lin D, Tang X, Xing J, Zhao J, Liang H, Li G. Application of peroxymonosulfate-based advanced oxidation process as a novel pretreatment for nanofiltration: comparison with conventional coagulation. Sep Purif Technol. 2019;224:255–64.

107. Thombre NV, Gadhekar AP, Patwardhan AV, Gogate PR. Ultrasound induced cleaning of polymeric nanofiltration membranes. Ultrason Sonochem. 2020;62:104891.
108. Epsztein R, Shaulsky E, Dizge N, Warsinger DM, Elimelech M. Role of ionic charge density in Donnan exclusion of monovalent anions by nanofiltration. Environ Sci Technol. 2018;52(7):4108–16.
109. Wang S, Li L, Yu S, Dong B, Gao N, Wang X. A review of advances in EDCs and PhACs removal by nanofiltration: mechanisms, impact factors and the influence of organic matter. Chem Eng J. 2021;406:126722.
110. Nair RR, Protasova E, Strand S, Bilstad T. Implementation of Spiegler¯ Kedem and steric hindrance pore models for analyzing nanofiltration membrane performance for smart water production. Membranes. 2018;8(3):78.
111. Su J, Chung T-S. Sublayer structure and reflection coefficient and their effects on concentration polarization and membrane performance in FO processes. J Membr Sci. 2011;376(1):214–24.
112. Rajendran RM, Garg S, Bajpai S. Modelling of arsenic (III) removal from aqueous solution using film theory combined Spiegler-Kedem model: pilot-scale study. Environ Sci Pollut Res Int. 2021;28(11):13886–99.
113. Ghazali NF, Razak NDA. Recovery of saccharides from lignocellulosic hydrolysates using nanofiltration membranes: a review. Food Bioprod Process. 2021;126:215–33.
114. Ali MEA, Kotp YH, Bosela R, Samy A, Awad S, Du JR. Enhancing the performance of TFC nanofiltration membranes by adding organic acids in polysulfone support layer. Polym Test. 2020;91:106775.
115. Sigurdardottir SB, DuChanois RM, Epsztein R, Pinelo M, Elimelech M. Energy barriers to anion transport in polyelectrolyte multilayer nanofiltration membranes: role of intra-pore diffusion. J Membr Sci. 2020;603:117921.
116. Peeters JMM, Boom JP, Mulder MHV, Strathmann H. Retention measurements of nanofiltration membranes with electrolyte solutions. J Membr Sci. 1998;145(2):199–209.
117. Bajpai S, Rajendran RM, Hooda S. Modeling the performance of HPA membrane for sulfate ion removal from ternary ion system. Korean J Chem Eng. 2019;36(10):1648–56.
118. Ortiz-Albo P, Ibañez R, Urtiaga A, Ortiz I. Phenomenological prediction of desalination brines nanofiltration through the indirect determination of zeta potential. Sep Purif Technol. 2019;210:746–53.
119. Kumar VS, Hariharan KS, Mayya KS, Han S. Volume averaged reduced order Donnan steric pore model for nanofiltration membranes. Desalination. 2013;322:21–8.
120. Roy Y, Warsinger DM, Lienhard JH. Effect of temperature on ion transport in nanofiltration membranes: diffusion, convection and electromigration. Desalination. 2017;420:241–57.
121. Wang R, Lin S. Pore model for nanofiltration: history, theoretical framework, key predictions, limitations, and prospects. J Membr Sci. 2021;620:118809.
122. Cooper J, Ye Y, Razmjou A, Chen V. High-value organic acid recovery from first-generation bioethanol dunder using nanofiltration. Ind Eng Chem Res. 2020;59(26):11940–52.
123. Caltran I, Rietveld LC, Shorney-Darby HL, Heijman SGJ. Separating NOM from salts in ion exchange brine with ceramic nanofiltration. Water Res. 2020;179:115894.
124. Almijbilee MMA, Wu X, Zhou A, Zheng X, Cao X, Li W. Polyetheramide organic solvent nanofiltration membrane prepared via an interfacial assembly and polymerization procedure. Sep Purif Technol. 2020;234116033.
125. Otero-Fernández A, Díaz P, Otero JA, Ibáñez R, Maroto-Valiente A, Palacio L, Prádanos P, Carmona FJ, Hernández A. Morphological, chemical and electrical characterization of a family of commercial nanofiltration polyvinyl alcohol coated polypiperazineamide membranes. Eur Polym J. 2020;126:109544.
126. Karimnezhad H, Navarchian AH, Tavakoli Gheinani T, Zinadini S. Incorporation of iron oxyhydroxide nanoparticles in polyacrylonitrile nanofiltration membrane for improving water permeability and antifouling property. React Funct Polym. 2019;135:77–93.
127. Álvarez-Quintana S, Carmona FJ, Palacio L, Hernández A, Prádanos P. Water viscosity in confined nanoporous media and flow through nanofiltration membranes. Microporous Mesoporous Mater. 2020;303:110289.
128. Malhotra M, Pal M, Pal P. A response surface optimized nanofiltration-based system for efficient removal of selenium from drinking water. J Water Process Eng. 2020;33:101007.
129. Rajendran RM, Garg S, Bajpai S. Economic feasibility of arsenic removal using nanofiltration membrane: a mini review. Chem Pap. 2021;75:4431–44.
130. Boussouga Y-A, Frey H, Schäfer AI. Removal of arsenic(V) by nanofiltration: impact of water salinity, pH and organic matter. J Membr Sci. 2021;618:118631.
131. Figoli A, Fuoco I, Apollaro C, Chabane M, Mancuso R, Gabriele B, Rosa RD, Vespasiano G, Barca D, Criscuoli A. Arsenic-contaminated groundwaters remediation by nanofiltration. Sep Purif Technol. 2020;238:116461.
132. Bouhadjar SI, Kopp H, Britsch P, Deowan SA, Hoinkis J, Bundschuh J. Solar powered nanofiltration for drinking water production from fluoride-containing groundwater – a pilot study towards developing a sustainable and low-cost treatment plant. J Environ Manag. 2019;231:1263–9.
133. Fujioka T, Ngo MTT, Makabe R, Ueyama T, Takeuchi H, Nga TTV, Bui X-T, Tanaka H. Submerged nanofiltration without pretreatment for direct advanced drinking water treatment. Chemosphere. 2021;265:129056.
134. Pica NE, Funkhouser J, Yin Y, Zhang Z, Ceres DM, Tong T, Blotevogel J. Electrochemical oxidation of hexafluoropropylene oxide dimer acid (GenX): mechanistic insights and efficient treatment train with nanofiltration. Environ Sci Technol. 2019;53(21):12602–9.
135. Pal P, Sardar M, Pal M, Chakrabortty S, Nayak J. Modelling forward osmosis-nanofiltration integrated process for treatment and recirculation of leather industry wastewater. Comput Chem Eng. 2019;127:99–110.
136. Giagnorio M, Ricceri F, Tagliabue M, Zaninetta L, Tiraferri A. Hybrid forward osmosis¯ nanofiltration for wastewater reuse: system design. Membranes (Basel). 2019;9(5):61.
137. Giagnorio M, Ricceri F, Tiraferri A. Desalination of brackish groundwater and reuse of wastewater by forward osmosis coupled with nanofiltration for draw solution recovery. Water Res. 2019;153:134–43.
138. Gönder ZB, Balcıoğlu G, Vergili I, Kaya Y. An integrated electrocoagulation–nanofiltration process for carwash wastewater reuse. Chemosphere. 2020;253:126713.
139. Vendrell-Puigmitja L, Abril M, Proia L, Espinosa Angona C, Ricart M, Oatley-Radcliffe DL, Williams PM, Zanain M, Llenas L. Assessing the effects of metal mining effluents on freshwater ecosystems using biofilm as an ecological indicator: comparison between nanofiltration and nanofiltration with electrocoagulation treatment technologies. Ecol Indic. 2020;113:106213.
140. Werner A, Rieger A, Helbig K, Brix B, Zocher J, Haseneder R, Repke J-U. Nanofiltration for the recovery of indium and germanium from bioleaching solutions. Sep Purif Technol. 2019;224:543–52.
141. Meschke K, Hansen N, Hofmann R, Haseneder R, Repke J-U. Influence of process parameters on separation performance of strategic elements by polymeric nanofiltration membranes. Sep Purif Technol. 2020;235:116186.
142. López J, Reig M, Vecino X, Gibert O, Cortina JL. From nanofiltration membrane permeances to design projections for the remediation and valorisation of acid mine waters. Sci Total Environ. 2020;738:139780.

143. López J, Reig M, Gibert O, Cortina JL. Increasing sustainability on the metallurgical industry by integration of membrane nanofiltration processes: acid recovery. Sep Purif Technol. 2019;226:267–77.
144. Yun T, Kwak S-Y. Recovery of hydrochloric acid using positively-charged nanofiltration membrane with selective acid permeability and acid resistance. J Environ Manag. 2020;260:110001.
145. López J, Reig M, Vecino X, Gibert O, Cortina JL. Comparison of acid-resistant ceramic and polymeric nanofiltration membranes for acid mine waters treatment. Chem Eng J. 2020;382:122786.
146. Reis BG, Araújo ALB, Vieira CC, Amaral MCS, Ferraz HC. Assessing potential of nanofiltration for sulfuric acid plant effluent reclamation: operational and economic aspects. Sep Purif Technol. 2019;222:369–80.
147. Motta Cabrera S, Winnubst L, Richter H, Voigt I, Nijmeijer A. Industrial application of ceramic nanofiltration membranes for water treatment in oil sands mines. Sep Purif Technol. 2021;256:117821.
148. Esteves T, Mota AT, Barbeitos C, Andrade K, Afonso CAM, Ferreira FC. A study on lupin beans process wastewater nanofiltration treatment and lupanine recovery. J Clean Prod. 2020;277:123349.
149. Tavangar T, Jalali K, Alaei Shahmirzadi MA, Karimi M. Toward real textile wastewater treatment: membrane fouling control and effective fractionation of dyes/inorganic salts using a hybrid electrocoagulation – nanofiltration process. Sep Purif Technol. 2019;216:115–25.
150. Tran TTV, Kumar SR, Lue SJ. Separation mechanisms of binary dye mixtures using a PVDF ultrafiltration membrane: Donnan effect and intermolecular interaction. J Membr Sci. 2019;575:38–49.
151. Ağtaş M, Yılmaz Ö, Dilaver M, Alp K, Koyuncu İ. Hot water recovery and reuse in textile sector with pilot scale ceramic ultrafiltration/nanofiltration membrane system. J Clean Prod. 2020;256:120359.
152. Santibáñez L, Córdova A, Astudillo-Castro C, Illanes A. Effect of the lactose hydrolysis on galacto-oligosaccharides mixtures subjected to nanofiltration: a detailed fractionation analysis. Sep Purif Technol. 2019;222:342–51.
153. Completo C, Geraldes V, Semião V, Mateus M, Rodrigues M. Comparison between microfluidic tangential flow nanofiltration and centrifugal nanofiltration for the concentration of small-volume samples. J Membr Sci. 2019;578:27–35.
154. Schmidt CM, Sprunk M, Löffler R, Hinrichs J. Relating nanofiltration membrane morphology to observed rejection of saccharides. Sep Purif Technol. 2020;239:116550.
155. Abdellah MH, Liu L, Scholes CA, Freeman BD, Kentish SE. Organic solvent nanofiltration of binary vegetable oil/terpene mixtures: experiments and modelling. J Membr Sci. 2019;573:694–703.
156. Cuhorka J, Wallace E, Mikulášek P. Removal of micropollutants from water by commercially available nanofiltration membranes. Sci Total Environ. 2020;720:137474.
157. Taheri E, Hadi S, Amin MM, Ebrahimi A, Fatehizadeh A, Aminabhavi TM. Retention of atenolol from single and binary aqueous solutions by thin film composite nanofiltration membrane: transport modeling and pore radius estimation. J Environ Manag. 2020;271:111005.
158. Giacobbo A, Soares EV, Bernardes AM, Rosa MJ, de Pinho MN. Atenolol removal by nanofiltration: a case-specific mass transfer correlation. Water Sci Technol. 2020;81(2):210–6.
159. Egea-Corbacho A, Gutiérrez Ruiz S, Quiroga Alonso JM. Removal of emerging contaminants from wastewater using nanofiltration for its subsequent reuse: Full–scale pilot plant. J Clean Prod. 2019;214:514–23.
160. Foureaux AFS, Reis EO, Lebron Y, Moreira V, Santos LV, Amaral MS, Lange LC. Rejection of pharmaceutical compounds from surface water by nanofiltration and reverse osmosis. Sep Purif Technol. 2019;212:171–9.
161. Cristóvão MB, Torrejais J, Janssens R, Luis P, Van der Bruggen B, Dubey KK, Mandal MK, Bronze MR, Crespo JG, Pereira VJ. Treatment of anticancer drugs in hospital and wastewater effluents using nanofiltration. Sep Purif Technol. 2019;224:273–80.
162. Xu R, Zhou M, Wang H, Wang X, Wen X. Influences of temperature on the retention of PPCPs by nanofiltration membranes: experiments and modeling assessment. J Membr Sci. 2020;599:117817.
163. Roy Y, Lienhard JH. A framework to analyze sulfate versus chloride selectivity in nanofiltration. Environ Sci Water Res Technol. 2019;5(3):585–98.
164. Kapsch AM, Farcet MR, Wieser A, Ahmad MQ, Miyabayashi T, Baylis SA, Blümel J, Kreil TR. Antibody-enhanced hepatitis E virus nanofiltration during the manufacture of human immunoglobulin. Transfusion. 2020;60(11):2500–7.
165. Ideno S, Takahashi K, Yusa K, Sakai K. Quantitative PCR evaluation of parvovirus B19 removal via nanofiltration. J Virol Methods. 2020;275:113755.
166. Roth NJ, Dichtelmüller HO, Fabbrizzi F, Flechsig E, Gröner A, Gustafson M, Jorquera JI, Kreil TR, Misztela D, Moretti E, Moscardini M, Poelsler G, More J, Roberts P, Wieser A, Gajardo R. Nanofiltration as a robust method contributing to viral safety of plasma-derived therapeutics: 20 years' experience of the plasma protein manufacturers. Transfusion. 2020;60(11):2661–74.
167. Kramer FC, Shang R, Rietveld LC, Heijman SJG. Influence of pH, multivalent counter ions, and membrane fouling on phosphate retention during ceramic nanofiltration. Sep Purif Technol. 2019;227:115675.
168. Arola K, Mänttäri M, Kallioinen M. Two-stage nanofiltration for purification of membrane bioreactor treated municipal wastewater – minimization of concentrate volume and simultaneous recovery of phosphorus. Sep Purif Technol. 2021;256:117255.
169. Thomson BM, Tandukar S, Shahi A, Lee CO, Howe KJ. Mineral recovery enhanced desalination (MRED) process: an innovative technology for desalinating hard brackish water. Desalination. 2020;496:114761.
170. Mohamad N, Reig M, Vecino X, Yong K, Cortina JL. Potential of nanofiltration and reverse osmosis processes for the recovery of high-concentrated furfural streams. J Chem Technol Biotechnol. 2019;94(9):2899–907.
171. Bush JA, Vanneste J, Cath TY. Comparison of membrane distillation and high-temperature nanofiltration processes for treatment of silica-saturated water. J Membr Sci. 2019;570:258–69.
172. Jeong K, Yoon N, Park S, Son M, Lee J, Park J, Cho KH. Optimization of a nanofiltration and membrane capacitive deionization (NF-MCDI) hybrid system: experimental and modeling studies. Desalination. 2020;493:114658.
173. Nativ P, Fridman-Bishop N, Nir O, Lahav O. Dia-nanofiltration-electrodialysis hybrid process for selective removal of monovalent ions from Mg2+ rich brines. Desalination. 2020;481:114357.
174. Ten Kate, AJB, Schutyser, MAI, Kuzmanovic, B, Westerink, JB, Manuhutu F, Bargeman G. Thermodynamic perspective on negative retention effects in nanofiltration of concentrated sodium chloride solutions. Sep Purif Technol. 2020;250:117242.
175. Yang R. Analytical methods for polymer characterization. 1st ed. Milton: Taylor & Francis Group; 2018.